The Double Seismic Zone of the Nazca Plate in Northern Chile: High Resolution Velocity Structure, Petrological Implications and Thermo-Mechanical Modelling

Catherine Dorbath[1], Muriel Gerbault[2], Gabriel Carlier[3], Michel Guiraud[3]

1: IRD UR154 and EOST, Université Louis Pasteur, Strasbourg, France.
2: IRD UR154, Departamento de Geologia, Universidad de Chile, Santiago, Chile, and LMTG UMR5563, Toulouse, France
3: CNRS, UMR 7160 (Minéralogie-Pétrologie) and MNHN, USM 201, Paris, France.

Abstract

This paper presents an interdisciplinary study of the Northern Chile Double Seismic Zone. First, a high resolution velocity structure of the subducting Nazca Plate has been obtained by a new double-difference tomography method. The double seismic zone (DSZ) is observed between 80 and 140 km depth and the two seismic planes are 20 km apart. Then, the chemical and petrologic characteristics of the oceanic lithosphere associated to this DSZ are deduced by using current thermal-petrological-seismological models, and are compared to pressure-temperature conditions provided by a numerical thermo-mechanical model. Our results agree with the common hypothesis that seismicity in both upper and lower planes are related to fluid releases associated to metamorphic dehydration reactions. In the seismic upper plane located within the upper crust, these reactions would affect material of basaltic (MORB) composition and document different metamorphic reactions occurring within high-P (> 2.4 GPa) and low-T (< 570°C) jadeite-lawsonite blueschists and, at greater depth (> 130 km), lawsonite-amphibole eclogite conditions. The lower plane lying in the oceanic mantle can be associated to serpentinite dehydration reactions. The Vp and Vs characteristics of the region in between both planes are consistent with a partially (~25-30 vol.% antigorite, ~0-10% vol. % brucite and ~4-10 vol. % chlorite) hydrated harzburgitic material. Discrepancies persist that we attribute to complexities inherent to heterogeneous structural compositions. While various geophysical indicators evidence particularly cold conditions in both the descending Nazca plate and the continental fore-arc, thermo-mechanical models indicate that both seismic planes delimit the inner-slab compressional zone around the 400°C (±50°C) isotherm. Lower plane earthquakes are predicted to occur in the slabs flexural neutral plane, where fluids released from surrounding metamorphic reactions could accumulate and trigger seismicity. Fluids migrating upwards from the tensile zone below could be blocked in their ascension by the compressive zone above this plane, thus producing a sheeted layer of free fluids, or a serpentinized layer. Therefore earthquakes may present either down-dip compression and down-dip extension characteristics. Numerical tests indicate that inner-slab compression is not only favored by the slab's thermal structure such as plate age. i) A weak ductile subduction channel, and ii) a cold mantle fore-arc both favor inner-slab compression by facilitating transmission of compressional stresses from the continental lithosphere into the slab. iii) Decreasing the radius of curvature of the slab broadens the depth of inner-slab compression, whereas iv) decreasing upper plate convergence diminishes its intensity. All these factors indicate that if indeed DSZs contour inner-slab compression, they cannot only be linked to slab unbending, but also to the transmission of high compressional stresses from the upper plate into the slab.

1- Introduction

Since Hasegawa et al. (1978) showed the existence of a double-planed deep seismic zone in the Northern Japan arc, more and more double seismic zones (DSZ) have been recognised in worldwide subduction zones like Tonga, New Britain, Kuriles, Kamchatka, Aleutians or Alaska (Peacock, 2001). Actually, a recent analysis of various subducting plates reveals the global prevalence of DSZ, which were found in segments of 16 subduction zones (Brudzinski et al., 2007). For these zones, the intermediate depth earthquakes (80 to 180 km) define two dipping planes separated by a distance increasing with plate age, from ~8 km for a ~12-My-old slab to ~30 km for a 160-My-old slab.

Seismicity in both upper and lower seismic zones occurs where stable hydrous minerals are predicted (Hacker et al., 2003b). Upper plane seismicity is linked to dehydration of metabasalts from the oceanic crust, and lower plane seismicity would be promoted by dehydration embrittlement of serpentinised mantle, e.g. antigorite (Hacker et al. 2003b; Yamasaki & Seno 2003; Brudzinski et al., 2007), with mantle hydration acquired by infiltration of seawater through outer-rise faults prior to subduction (Seno & Yamanaka, 1996; Peacock, 2001).

Despite this observation of a first order dependancy of DSZ separation on plate age by Brudzinski et al. (2007), the mechanical cause for their occurence remains misunderstood. Numerous authors have suggested that DSZs are caused by unbending of the lithosphere after passing the position of maximum curvature (e.g. Engdahl and Scholz, 1977; Isacks & Barazangi, 1977; Wang, 2002), inducing upper plane compressional earthquakes in the top part of the slab, and lower plane down-dip tension earthquakes in its bottom part. But many slabs are nearly planar where the lower plane seismicity continues (e.g. Fujita & Kanamori, 1981; Abers, 1992), suggesting that a continuous stress acts on the slab long after it has passed the point of unbending. Fault-plane solutions are also found poorly consistent with plate bending and unbending about a neutral fiber (e.g. Peacock, 2001). A while ago, Fujita and Kanamori (1981) had suggested that double seismic zones are observed in slabs for which the plate sinking rate (function of its age) differs from surface plate convergence velocity, sufficiently to generate stress-segmented seismic zones. When such slabs are on average, neither dominantly in tension or compression, seismogenic deviatoric stresses may be generated by local factors such as, for example, thermal stresses or compressional stresses transmitted from the upper plate into the slab.

It is known that a double seismic zone also exists in the subducting Nazca Plate beneath Northern Chile, just south of the Arica elbow. Yet, seismic data lead controversal DSZ characteristics. In this area, the 50 Ma old Nazca plate (e.g. Cande & Haxby, 1991) is subducting beneath the South American plate at a rate of 84 mm/yr. From a microseismic field experiment between 20 and 24°S, Comte and Suarez (1994) observed, at depths of 80 to 150 km, two families of events with opposite focal mechanisms; the average separation between these two sets of events is about 15 km, suggesting a double layered slab. Nevertheless, the high quality results from the PISCO'94 experiment, deployed in the same region, gave no evidence for a double seismic zone (Graeber and Asch, 1999). On the other hand, locally recorded events between 18.5 and 19.5°S display, at depths greater than 100 km, two distinct planes separated by 20 to 25 km, with an extreme variability of the focal mechanisms observed in both planes (Comte et al., 1999). About 300 km south, around 22°S, Rietbrock & Waldhauser (2004) used the double-difference algorithm (hypoDD, Waldhauser, 2001) to evidence a 9 km thick DSZ at 80-130 km depth, and with predominant extensional events in both upper and lower planes.

Recently, Zhang et al. (2004) provided high resolution constraints on the petrological processes involved in double seismic zones by studying the subduction beneath Northern Honshu, using an improved double-difference tomography method, tomoDD. Where previous seismic tomography studies lack information, particularly on the velocity structure of the deeper part of the slabs, this method is able to produce more accurate velocity images in the region near the sources (Zhang & Thurber, 2003). In this paper, we first apply this new double-difference tomography code to the Arica zone data (section 2.1), to obtain a detailed velocity model of the subducting Nazca plate where a double seismic zone has been observed (section 2.2). From this velocity model we then compare our results with those obtained for Honshu, and discuss the implications on petrological compositions when using Hacker & Abers (2004) calculation scheme (section 2.2). Amongst these pecular implications, we argue for a cold thermal

environment, and therefore develop in section 3 a thermo-mechanical numerical model of the Northern Chile subduction zone. We start this section 3 by reviewing the litterature, surface heat-fluxes, thermal models and geophysical data of the area (section 3.1). We then expose our numerical approach, with initial conditions that are based on these data, and results that display the evolution of the subduction zone towards a transient thermo-mechanical state (section 3.2) that accounts for elastic-viscous and brittle behaviour. We then reconsider our initial petrological results in comparison to the pressure-temperature conditions obtained with these thermo-mechanical models (section 3.3), and finally display alternate thermo-mechanical models, in which we show that not only temperatures but also stresses play a crucial rôle in the width and depth of DSZs (section 3.4). This paper is consequently rather dense as it contains a number of interdisciplinary considerations, but it is also this interdisciplinary approach that provided us with a global view of the processes in play, allowing to frame the pecular conclusions we propose.

2- High resolution velocity structure

2.1- Data and method

From June to August 1996, a dense temporary seismic network was deployed in the Arica region from the coast to the Bolivian border, between the Peruvian border and 19°20'S. This short period array of 24 vertical and 10 three-component stations complemented the Arica permanent network of 9 stations (Figure 1). P and S arrival times in these 43 stations were used to determine hypocentral locations. A description of the network and location process may be found in Comte et al. (1999). In this paper, only the travel times of the very best located earthquakes recorded during this experiment, complemented by those recorded by the permanent network from January 1996 to December 1997, have been used.

We kept 2052 events, which met all the following restrictive criteria: number of readings higher than 10 including 2 S, distance to the nearest station lower than depth, rms lower than 0.25, azimuthal gap lower than 300 and conditioning factor lower than 100 (Figure 1). We prefered using these few very selected events instead of numerous redundant and poorly located events that will introduce noise in the data and degrade the results. We obtained about 36,000 absolute travel times (~55% of P waves), from which we constructed 171,000 differential travel times for events pairs. We used the same interevent maximal distance as Zhang et al. (2004), e.g. 10 km at common stations, in order to reduce the velocity model dependancy on double-difference earthquake relocation.

In addition to the hypocentral relocations, we simultaneously solve the P and S wave velocity structure at each grid node. The chosen inversion grid is presented on Figure 1 in map view. The origin of the grid is at X=69°W, Y=18°S, Z=0 km. Rotation of the reference frame to N77°E corresponds to the convergence direction of the Nazca plate underneath South America at that latitude. The distance between nodes is 10 km in the three directions, down to 160 km, below the maximal depth of the hypocenters in this area. We first inverted these travel-times data for a 1D velocity model, starting from the very simple model previously used for the standard hypocentral location procedure in Northern Chile (in blue in Figure 2), and interpolating it in 17 regularly spaced layers defined between 0 and 160 km. The final model (in red in Figure 2) is very close to the model obtained in the same geographic area by Comte et al. (2004) from a 1D inversion of 10,000 events recorded by 13 stations. In particular, the high velocity zone at ~50 km depth and the low velocity zone between 120 and 150 km are observed on both models. The obtained velocities were used as initial velocities for the 3D tomoDD inversion.

Numerous tests have been performed to check the robustness of the 3D solution. As we ran tomoDD in LSQR mode, we controlled the damping at each iteration by keeping the condition number value between 40 and 50 (Waldhauser, 2001). Various interevent maximum distances have been tested, and show that inversions using different cutoffs give similar results. Several inversions were performed with various strategies of weighting absolute data relatively to differential data. Our final weighting scheme first a priori down-weights the differential data, in order to obtain a large-scale velocity model from the absolute data. In a second step, we favor the differential data, in order to improve the location of nearby events and refine the velocity model. In the last set of iterations, we then re-weight the data, according to misfit and event separation, in order to remove or down-weight outliers. Various distances between the grid nodes have been tested in order to get the best trade-off between grid spacing and data

resolution. The square root of the derivative weight sum (DWS) along profile P2 (Figure 1) is presented for Vp and Vs models in Appendix 1 (A) and (B) respectively. Thereafter, the iso-value 10, considered as the limit for resolved structures, is drawn on all figures. The influence of the chosen initial velocity model on the final velocity structures is presented in Appendix 1. Figures (C) and (D) present the results obtained for Vp and Vs starting from the final 1D model (red dots, Figure 2), whereas figures (E) and (F) present the results obtained starting from the initial model (blue dots, Figure 2). We see that the influence of the initial velocity model is minor.

Three resolution tests are presented in Appendix 2 for Vp, and Appendix 3 for Vs. In each test, the calculated synthetic absolute and differential travel-times are included only for the same data distribution as for the real data. Following the standard procedure, we add uniformly distributed random noise to the synthetic data, in the interval +/- 0.025s for P waves and +/- 0.05s for S waves. The inverted models are obtained with the same inversion scheme as the real data set and starting from the same 1D final model. Similar resolution tests have been performed in DSZ contexts by Zhang et al. (2004) or Shelly et al. (2006).

- Checkerboard test: the synthetic input P- and S-wave velocity models consist of 20 x 20 x 20 km patches (covering 2 nodes in horizontal and vertical directions) with velocities alternatively +5% and -5% compared to the normal starting model (Appendices 2 and 3, Figures A). Recovered P and S wave models are presented in figures B of Appendices 2 and 3. It is clear that P and S wave velocities features are well resolved in the subduction zone. The features are recovered in position and magnitude for the upper plane, but with a bit lower amplitudes for the lower plane. In the test presented here, the diagonal step of the grid (45°) differs from the dip of the slab (35°), and the colour alternance of diagonal high/low velocities, if similar to our results for Vp, is opposite to our results for Vs. The continental lithosphere area is poorly resolved down to 80 km to the east, a result that is evident in both following tests.
- Restoring resolution test (Zhao et al, 1992): this test estimates the ability of the real data to recover the model obtained from the inversion. The input velocity models, which are the inverted true models, are shown in Figures C of Appendices 2 and 3, and the corresponding recovered velocity models are shown in Figures D. The velocity features of the subduction zone are well recovered in position and magnitude within the upper plane. Within the lower plane, the recovered velocities are decreased. Nevertheless, this test shows that if the observed anomalies exist, the dataset enables to recover them.
- the last test starts from an input model without any velocity anomaly (Appendices 2 and 3, Figures E). Except in the easternmost part of the recovered velocity models (F), no marked anomaly is observed. This third test shows that, if no anomaly exists, our data do not generate it, therefore if no low Vp/high Vs zone is present, the inversion does not generate it as an artifact.

2.2- Tomography results and discussion

We present on Figure 3 three cross sections through our final velocity models Vp and Vs and through the relocated hypocentres along profiles P1 (Y=-20 km), P2 (Y=-60 km) and P3 (Y=-100 km) (Figure 1). These sections are representative of the slab in Northern Chile, as other cross sections show similar features. Figure 4 displays Vp and Vs zoomed on the DSZ along profile P2, which is in the center of the studied area and thus the best resolved. On both figures, the white lines correspond to the iso-value 10 of the square root of derivative weight sum, considered as the limit for resolved structures. The Vp/Vs model is obtained by simple division of Vp by Vs models in regions where both models are resolved. Appendix 1 (A) and (B) shows that the resolution of both models allows to calculate it. However, it is important to keep in mind that such direct division can carry instabilities.

At intermediate depth (80–140 km) the double seimic zone is situated under our seimic array, well defined and reasonably well resolved. Both seismically active planes are 5 to 10 km thick, with a clear separation of 20 km (Figure 3). In this part of the velocity model (Figure 4), the planes present outstanding distinct features which are summarized in Table 1.

2.2.1- The Fore-arc mantle:

In the fore-arc mantle below about 40 km and above ~110 km depths, Vp values are in the 7.5-8

km/s range, and Vs values are in between 4 and 4.5 km/s, very similar to the Honshu region. The Vp/Vs values do not present any large size anomaly, but oscillate from about 1.75 to 1.85. In contrast, in the Honshu region between 20-90 km depth below the volcanic arc, Vp/Vs values are homogeneously high (~1.8-1.9), and are interpreted by Zhang et al. (2004) to be associated with melt and water inclusions transported through hydraulic fractures from the slab where dehydration reactions occur. These dehydration reactions are attributed to the occurrence of serpentinized peridotite containing melt-filled pores, and are consistent with thermal studies of the Honshu region indicating temperatures above ~700°C. In Northern Chile, however, several studies indicate that the fore-arc mantle is significantly colder, such as thermal models by Honda (1985) or Springer (1999), and flexural rigidity estimations by Tassara (2005) and Tassara et al. (2007). In addition, geophysical studies show an exceptionally low seismic attenuation (e.g. Haberland et al., 2003, more details in the thermal structure section 3.2), and a specific seismic anisotropy pattern (Kneller et al., 2005, 2007, details in section 3.2), also indicative of low temperature and high stress environment. Therefore, many lines of evidence show that the Northern Chile forearc mantle differs from other warm subduction zones that are characterised by extensively serpentinized, melt-equilibrated fore-arc mantle (e.g. Kelemen et al., 2003; Hyndman & Peacock, 2003, see also discussion in section 3.3).

The geological evolution of the south Peruvian and north Chilean fore-arc is complex as indicated by the occurrence of Precambrian blocks (i. e. Arequipa Massif) preserved within predominantly volcanic Phanerozoic material. Thus, the fore-arc-mantle is probably also complex and predominantly composed of more or less metasomatized harzburgitic material, for which general compositions systematically lead to high Vp (> 8. km/s) and Vs (> 4.6 km/s) values. At depths of 40-110 km, our recorded velocity values (Vp = 7.5-8.0 km/s ; Vs = 4.0-4.5 km/s) militate for a partially hydrated harzburgitic fore-arc mantle, when deduced from petrological simulations (1.2-2.9% H_2O, 10-24% modal antigorite; Hacker et al. 2003a; Hacker & Abers, 2004). These petrological simulations are also consistent with the presence of a cold mantle in Northern Chile (<600°C).

2.2.2- The DSZ, petrological candidates deduced from tomographic results

Our results (Table 1) are very close to the slab velocity structure obtained by Zhang et al. (2004) in the Honshu DSZ at 39°N, and slightly different from those obtained by Shelly et al. (2006) at 37°N. In Honshu, the old (130 Ma) Pacific plate subducts beneath the Eurasian plate at 91 mm/yr (DeMets et al., 1990). The two seismic planes of the DSZ are separated by ~30 km at intermediate depths of 50–140 km.

In New Zealand, the observed DSZ are not as clear as in Japan, however the velocity structure obtained by Zhang (2003) with tomoDD in the Wellington region, may be compared to the Chilean results. Nevertheless in this region, the Pacific plate is about 120 Ma old, and the subduction process is much slower (42 mm/yr). Both seismic planes are detected at shallower depths, from 50 km to only 80 km due to land-sea limits, and are separated by ~10 km. The results of these three tomoDD studies are summarized in Table 2. The structure of the Hikurangi subduction zone beneath the central North Island, New Zealand, to the north of Zhang's study (Reyners et al., 2006) was also obtained by simultaneous inversion for both hypocentres and the 3-D Vp andVp/Vs structure (Thurber 1983, 1993). Results define the DSZ down to 130–140 km depth. Earthquakes in the lower plane are generally associated with regionally high Vp values, and a specifically low Vp/Vs, which is similar to lower plane earthquakes in Northern Honshu.

Focal mechanisms would help identifying the physical processes and metamorphic reactions involved in Northern Chile DSZ. Focal mechanisms constructed for the events recorded during the 1996 campaign have been presented by Comte et al. (1999). For the present study, we used our relocated events to construct focal mechanisms when possible. Only 45 solutions were constrained, among which 41 located in the upper plane, and 4 remaining in the lower plane. Our results do not differ from those obtained by Comte et al. (1999): fault plane solutions for these intermediate depth events vary significantly, even between nearby events. The very few events associated to the lower subduction plane also present an extreme variability (with both tensional and compressional mechanisms). Finally, polarities read from the very few earthquakes located in between both planes do not enable to draw any reliable mechanism. Such results were also observed by Abers (1992) in the Aleutian DSZ.

In order to assess the petrological compositions consistent with our tomographic data, the velocities proposed and discussed hereafter have been computed by averaging the values obtained in the central part of our model for the same area of the DSZ (upper plane, lower plane, and region in between), from P1 to P3 (Figure 1). Mineral rock compositions involved in upper and lower planes, and in between, are obtained by using Hacker & Abers's procedure (2004). For suitable Vp velocity data, we have selected rock compositions displaying the Vs velocities that most closely approximate the observed data. Then, the results are compared with available, independent petrogenetic data.

2.2.3-The upper plane

The upper plane of earthquakes in Northern Chile lies in a region of relatively low Vp (7.7 km/s) and normal Vs (4.6 km/s) values, thus relatively low Vp/Vs ratio (~1.67) (Table 1), from 80 to 130 km depth. Between 80 km (~2.4 GPa) and 140 km (~4.5 GPa) depth and, for rocks of basic composition (MORB), mineral velocities estimated by using the calculation scheme of Hacker & Abers (2004) imply mineral assemblages of relatively low Vp and high Vs values and, relatively high Vp and low Vs values, respectively for each depth range. Common minerals at such pressure and temperature are coesite, jadeite, kyanite and garnet, that show high Vs (>4.6 km/s) but also high Vp (>7.8 km/s) values. Therefore, whatever their respective modal proportions, these minerals must necessarily be associated to amphibole and/or chlorite, which significantly decrease the bulk-rock Vp values. Conversely, the observed low Vp velocity values preclude anhydrous metabasic rocks such as eclogite. Velocity simulations with Hacker & Abers (2004) tables agree with this conclusion.

Petrogenetic grids modelling high pressure metabasic rocks (CNFMASH system + silica phase and H_2O in excess) provide additional constraints (e.g., Clarke et al., 1997; Carson et al., 1999). In theses systems, at temperatures above 550°C, garnet and clinozoisite occur at the expense of chlorite and lawsonite, respectively. In contrast at low temperatures (<570°C), chlorite coexists with lawsonite, amphiboles and omphacite over a large pressure domain (e.g., lawsonite is stable above 1.6 GPa at 550°C). Since the relatively low Vp values of Northern Chile upper seismic plane imply the presence of chlorite and amphibole rather than garnet and clinozoisite, we propose that the involved mafic metamorphic rocks are characterized by low temperature (<570°C) mineral assemblages in presence of water. Petrological simulations using low temperature (500°C) and lawsonite-omphacite-amphibole-chlorite assemblages with 4.0-5.7 wt % H_2O and, at greater depth, lawsonite amphibole eclogite with 3.0 wt % H_2O (Hacker & Abers, 2004), provide Vp values that are close to observations.

Accordingly, we suggest that between 80 and 140 km depths, the seismic upper plane in Northern Chile is related to fluid release associated to metamorphic reactions occurring within jadeite-lawsonite blueschists and, at greater depth, under lawsonite-amphibole eclogite conditions. Note that these conditions occur at relatively low temperature (<570°C), consistent with indications of the cold state of the North Chilean subduction zone (see section 3.1).

2.2.4 -The intermediate zone

In between both seismic planes of the Northern Chile DSZ, mean Vp values are high (8.5 km/s), mean Vs values are slightly low to normal (4.5 km/s), leading a high Vp/Vs ratio (~1.8) (Table 1). Nevertheless, we observe a global decrease of the velocity values with depth, from [Vp ~8.8, Vs ~4.7] at ~80 km depth, to [Vp ~8.3, Vs ~4.4] at ~130 km depth. Vp values as high as 8.8 km/s are indicative of unmetamorphosed or metamorphosed harzburgite composition (Hacker et al., 2003a) under very high pressure (above 4.5 GPa for unmetamorphosed harzburgite, above 7 GPa for metamorphosed harzburgite), much greater than those inferred from the lithostatic conditions of the intermediate zone of Northern Chile(< 3.5 GPa). Simulations using Hacker & Abers (2004) indicate that, at 80 km depth and temperature <500°C, observed mean Vp values are consistent with anhydrous or slightly hydrated harzburgitic material (<0.6 wt% H_2O, ~10 vol. % antigorite). At 130 km depth, observed Vp values of 8.3 km/s are consistent with a similar material of water content up to 1.2 wt% (~10 vol. % antigorite) at low temperature (300°C) and 0.6 wt% (~5 vol. % antigorite) at higher temperature (600°C).

2.2.5-The lower plane

In Northern Chile, the lower plane of seismicity is characterized at all depths down to 130 km, by low Vp values (7.4 km/s), high Vs values (4.7 km/s), and very low Vp/Vs ratio (~1.57) (Table 1). Similar data have only been reported in the lower plane of Wellington DSZ, New Zealand (Zhang, 2003; Table 2). Such results have been generally attributed to serpentinites or chlorite-bearing harzburgites. However, at depths greater than 80 km (above ~2.5 GPa), occurrence of fully serpentinized rocks (15 wt% H_2O) is ruled out because they display too low Vp values (<6.2 km/s) with respect to the observed data of Northern Chile. Better results are obtained when partially hydrated harzburgite compositions are considered (5-7 wt% H_2O, with ~25-30 vol.% antigorite, ~0-10% vol. % brucite and ~4-10 vol. % chlorite, from petrological simulations,). At considered depths and in order to maintain relatively high Vs, such compositions imply that temperature probably does not exceed 500 °C in brucite-bearing or, depending on water activity, 500-650°C in brucite-free assemblages (see, i. e., Hacker et al., 2003a; Perrillat et al., 2005).

In conclusion, like for other worldwide DSZs, Northern Chile lower plane seismicity can be ascribed to dehydration reactions occuring within partially hydrated harzburgites. As noted above, the most probable involvement of brucite breakdown in these dehydration reactions and the fact that water activity is probably <1, implies that temperatures do not exceed 600°C.

Serious limitations to previous interpretations arise when considering the observed Vs values and Vp/Vs ratios (Table 1). Even worse, no mineral assemblage displaying both observed Vp and Vs values can be simulated using Hacker & Abers's calculation tables. The simulations systematically result in mineral assemblages displaying higher or lower Vs velocity for a suitable Vp velocity and vice versa. Such discrepancy may be ascribed to various parameters such as the presence of more complex oceanic crust or mantle compositions, occurrence of free-fluid phases (i.e., Nakajima et al., 2001; Hacker et al., 2003a), pore geometry (i. e., Takei, 2002), reaction kinetics (Evans, 2004; Perrillat et al., 2005), suitable mixing models used to convert velocity data in mineral composition (i. e., Ji & Wang, 1999), or medium to large scale rock heterogeneity (lattice preferred orientations, compositional layering; Ji & Wang, 1999).

Contribution of metamorphic sediments and/or greywackes within the subducting upper crust, as proposed for the Wellington DSZ, New Zealand (Zhang, 2003), could drastically reduce Vp/Vs ratios (Christensen, 1996). However, such a hypothesis is unlikely in Northern Chile because the subducting Nazca plate is known to have experienced very few pelagic deposits (< 850 m; Prince & Kulm, 1975). This feature is a direct consequence of the arid climate affecting the southwest intertropical coast of South America (e.g. Lamb & Davis, 2003, and references therein).

Petrological diversity in mantle material is rather limited. Nevertheless, addition of magnetite and clinopyroxene (diopside +jadeite) tend to increase the Vs values of the partially hydrated harzbugitic material used in our similations. Occurrence of magnetite is common in serpentinized rocks where it reaches up to 10 vol. % of the rock (i. e., Coleman & Keith, 1971). Significant amounts of clinopyroxene (> 8 vol. %) suggests that lherzolitic or wehrlitic layers could be interstratified within the harzburgitic material, a feature observed in some ophiolitic complexes that are considered to be typical of oceanic lithosphere (i. e., Oman ophiolites; Ceuleneer et al., 1988; Benn et al., 1988; Takazawa et al., 2003). This presence of clinopyroxene-rich layers in harzburgitic materiel brings up an another problem generally not considered in large-scale models (i. e., Hacker et al., 2003a, b; Hacker & Abers, 2004) : rock heterogeneity. The main characteristic of natural outcrops of mafic or ultramafic materials is their textural heterogeneity (i. e., Ceulener et al., 1988; Benn et al., 1988; Clarke et al., 1997; Carson et al., 1999; Takazawa et al., 2003). For example, jadeite-lawsonite blueschists and eclogites commonly exhibit metric, decametric or kilometric eclogitic, gabbroic lenses or layers, and peridotites generally contain pyroxenitic layers or dykes. In addition, some layers are more intensively deformed whereas others are less deformed (i. e., gabbroic or eclogitic lenses in blueschists, serpentinite layers in peridotites). Such features introduce significant anisotropy that could have important consequences on measured seismic velocities. In particular, it is remarkable that the Northern Chile DSZ lower plane displays Vp velocity values indicative of partly serpentinized peridotite (7.4 km/s) but Vs velocity values typical of anhydrous peridotite (4.7 km/s). The possibility that these data represent a fully serpentinized matrix containing

anhydrous harzburgite lenses or layers should be explored. Nevertheless, such a hypothetical concept needs to be experimentally tested.

Many authors (i.e., Nakajima et al., 2001; Takei, 2002; Hacker et al., 2003a,b) suggest that the presence of free H_2O-rich fluids phases can explain low Vp/Vs ratios. The occurrence of water in excess is certainly required by the modelling of amphibole-rich eclogitic rocks in Carson et al. (1999). Hydrous minerals, mainly chlorite, hornblende, epidote or lawsonite for mafic compositions, and antigorite, chrysotile, talc-like phase, or chlorite for ultramafc compositions are the source of the water released during prograde metamorphism. Discontinuous dehydration reactions and/or entrapment of water by physical processes during continuous dehydration could lead to the observed low Vp/Vs, and hence favor seismicity. Kinetics is an important factor that can affect the modeling. Petrogenetic grids are based on equilibrium thermodynamics. Yet, as the slab moves downwards, rapid changes in P and T can lead to kinetics driving reactions. Experiments by Perrillat et al. (2005) suggest that antigorite could breakdown at temperatures much below equilibrium petrogenetic grids (e.g. 520°C at 4GPa), thus consistent with release of water at low temperature, especially if fluid is taken out from the medium at the same rate as it is produced. Jung et al. (2004) have also shown that antigorite breakdown under shear stress does not follow equilibrium thermodynamics, and that dehydration embrittlement could be the process for continuous dehydration.

Another parameter that can significantly affect the rock Vp/Vs ratios is the pore geometry (Watanabe, 1993; Takei, 2000, 2002). For example, a specific pore configuration (i.e., tube geometry, equilibrium geometry, Watanabe 1993) corresponding to low hydration and water-undersaturated pores could be responsible for the observed velocities in the intermediate zone of the DSZ.

All our previous petrological interpretations of seismic velocities are based on data provided by Hacker et al. (2003a) and Hacker & Abers (2004), for which oceanic lithosphere materials are assumed restricted to an average MORB composition for the crust and an average harzburgite composition for the mantle. In order to explain our measured seismic velocities, we had to assume very specific compositional characteristics, and especially very cold conditions. Obviously other parameters such as rock heterogeneity and fluid configurations still require additional investigations in order to accurately evaluate their relative contribution. Meanwhile, an attempt to provide additional constraints is made in the following section, first by presenting the thermal and geophysical characteristics of both the subducting and the overriding plates, and then by developing thermo-mechanical models of the Northern Chile subduction zone.

3-Thermo-mechanical modelling

The idea is to setup a model with “reasonable” initial thermal and rheological structure, close to the Northern Chile conditions, and to record stress build-up and propagation of deformation when applying upper plate convergence and basal slab-pull, over a relatively short-time scale of 2 Ma. We present first the available data on the thermal structure of the region (section 3.1), referring to surface heat-flow measurements, existing thermal studies, and geophysical data. We then describe our numerical thermo-mechanical approach (section 3.2), which differs from standard thermal models of subduction zones. A reference model is then presented, illustrating the general dynamics of deformation, resulting from specific initial conditions. With this model, we discuss the Pressure-Temperature specificities for the Northern Chile DSZ (section 3.3). Finally, we illustrate with alternate models how the oceanic and continental thermal structures, the subducting channel rheology, and relative plate convergence, all affect these Pressure-Temperature conditions (section 3.4).

3.1- *Thermal structure in Northern Chile inferred from data*

Considering existing thermal studies of the Northern Chile subduction zone, we first recall the heat-flow data, studied by Springer & Forster (1998), who combined existing values (e.g. Hamza & Muñoz, 1996) with bore-holes data. The mean heat-flow density along a W-E generalized lithospheric structure shows the following trends: (1) Within the oceanic Nazca Plate low values of about 30 mW/m^2 occur in

the region of the Peru-Chile country boundary: these are low compared to the 70mW/m^2 deduced from a 50 Ma old plate cooling model. Springer & Forster (1998) explained this value by a probable faster cooling resulting from heat convection compared to pure heat conduction models. (2) A minimum heat-flow density of about 20 mW/m^2 is observed in the Coastal Cordillera, which would reflect cooling in the continental crust as a result of the subduction of oceanic lithosphere. Values increase toward the fore-arc region to 40-60 mW/m^2. (3) Heat flow varies from about 50 to 180 mW/m^2 in the area of the magmatic arc (sparse and equivocal) and the Altiplano. This large variability is interpreted by Springer & Forster (1998) as heat sources resulting from isolated magma chambers at shallow depths (~10km), in agreement with geological and geophysical information (see review in Schilling et al., 2006). (4) High values of about 80 mW/m^2 are typical for the back-arc region of the Eastern Cordillera, attributed to either doubling of the crust or rise of the asthenosphere. (5) Heat flow density is about 40 mW/m^2 in the Subandean Ranges and Chaco Basin, somewhat lower than the 50-60 mW/m^2 of the adjacent Brazilian Shield farther to the east (Hamza & Muñoz, 1996).

Geophysical investigations also give insight on the thermal structure of Northern Chile. We summarize here a review by Schilling et al., (2006). From magnetotelluric investigations, the volcanic arc does not appear as a conductive feature along the three MT profiles carried north of 21°S, but show instead a low conductivity zone, and very low conductivity in the fore-arc beneath the Coastal Cordillera, extending into the upper mantle (e.g. Brasse et al., 2002). However, there is a broad and intense anomaly in the mid-crust beneath the plateau at least 40-50 km deep (note that this is more than 350 km east of the trench), with evidences for a conductive root reaching the upper mantle, possibly representing the mantle wedge (Brasse, 2005). Seismic waves through the fore-arc crust indicate a cold crust containing only minor free fluids, and Qp tomography shows no indication of a fluid "curtain" extending from the descending slab into the fore-arc region. Some regions of the fore-arc show extremely low attenuation, indicative of a strong, cold lithospheric block (e.g. Haberland et al., 2003; Schurr & Rietbrock, 2004). This may impede magma generation, and explain the observed shift of the volcanic arc to a depth to the top of the slab reaching 110-130 km (e.g. global study by Syracuse & Abers, 2007).

The thermal structure of our numerical model should thus be constructed to comply with these data, and will be mostly based on previous thermal models developped by Springer (1999), and gravity models by Tassara et al (2006). This setup will be described in detail further in section 3.2.2, after having first presented our general numerical approach.

3.2- The thermo-mechanical modelling approach

We do not wish to account for full thermo-dynamical modeling of subduction processes in Northern Chile, for various reasons: 1) this subduction zone has been ongoing for almost 80 millions of years with still debated alternances of extensional and compressional upper plate arc regimes. For example, the very characteristic Altiplano feature that has built on the upper plate obviously indicates specific deep structural properties, and its rise, linked with the formation of the Arica elbow, is still debated to have occurred since either within the last 10 Myrs or 35 Myrs ago (e.g. Roperch et al., 2006, and references therein). 2) full thermo-mechanical models have already been published by Sobolev & Babeyko (2005, 2006), over a time duration of about 20 Myrs. Since in fact, a number of geophysical data and conceptual models of the present day structure of the Northern Chile margin exist, instead in this study, we wish to reproduce on a relatively short-time scale of about 2 Myrs, specific deformation and stress patterns surrounding the subduction zone interface. Therefore, we start from an hypothetical thermal structure, a geometrical structure and a rheological layering, that are built as close as we can to available published information, and which, implicitely, assume a relative thermal steady state and dynamical equilibrium of the forces in play.

We use a Lagrangian approach that simulates elastic-viscous-brittle behavior, Parovoz (Poliakov & Podladchikov, 1992), a 2D finite-differences numerical code based on the FLAC technique (Cundall & Board, 1988). It resolves differential equations alternately, with the output for the solution of the equations of motion used as input to the constitutive equations for a progressive, time-explicit, calculation. FLAC is based on a quadrilateral mesh formed by superimposing two constant stress/constant strain triangular finite elements. Each element behaves according to prescribed stress/strain constitutive

laws in response to kinematical boundary conditions: Mohr-Coulomb non-associative elasto-plasticity is combined with temperature-dependent visco-elasticity (Maxwell) so that locally, the minimum of both stresses is chosen. Accounting for elastic-brittle-ductile properties permits to model formation of faults or shear zones and lithospheric extension and collision (e.g. Poliakov et al., 1994; Lavier et al., 1999; Burov & Poliakov, 2001; Gerbault et al., 2003). The free upper surface boundary allows to adequately resolve for surface processes, which are accounted for with a diffusion equation with variable coefficient (Table 3). The basic equations of motion and heat transport in Lagrangian formulation for Parovoz can be found in a number of publications (e.g. Burov et al., 2003; Gerbault et al., 2003; Le Pourhiet et al., 2004; Yamato et al., 2007). The heat transport equation accounts for heat conduction, radioactive and shear heating, while heat advection is accounted for by the displacements of the Lagrangian grid. This version of Parovoz does not account for phases reactions and subsequent density evolution, and employs a remeshing technique using passive markers similar to Yamato et al. (2007). See appendix 4 for more details.

3.2.1- Rheologies and boundary conditions

The model (Figure 5) simulates an area 300 km deep by 1800 km wide, comprising a flexuring oceanic plate dipping at 35°. With 900 x 150 grid elements, horizontal resolution is 2 km, and vertical resolution decreases downwards from 1 to 4 km. Geometrical, rheological and thermal properties are summarized in Tables 3, 4, 5. Elastic, brittle and power-law creep parameters are chosen according to various sources from rock mechanics extrapolated to the lithospheric scale (e.g. Kirby et al., 1996; Rannalli, 1995, and references therein), and combined with the known special conditions for the Andes (e.g. Springer, 1999; Tassara, 2005; Sobolev & Babeyko, 2005). Composition and densities are defined mostly according to the recent three-dimensional density model from Tassara et al. (2006), who compiled appropriate characteristics of the Chilean Andes.

The following heterogeneities are inserted (see Tables 4, 5). First, in the continental crust (various red to brown colours in Figure 5): the upper crust is supposed to be of weak composition in the Bolivian fore-land (e.g. Sobolev & Babeyko, 2005), as opposed to the fore-arc crust, which is of rather mafic composition, coherent with geophysical data and geological history (e.g. flexural rigidity study by Tassara, 2005, 2006; seismology and magnetotellurics reviewed for example by Schilling et al., 2006; geology indicating long-lived arc magmatism, Lucassen et al., 2001). The Altiplano domain is characterised by a pre-thickened lower crust (65 km with respect to 35 km elsewhere), which has a more felsic behaviour (e.g. Lucassen et al., 2001; Beck & Zandt, 2002).

Second, the subduction channel, defined 10 km thick, is composed of three portions: the upper 10 km mimick unconsolidated oceanic crust, with a plagioclase rheology and a moderate friction angle of 5°. Below, weaker wet granite rheology is employed (this choice is discussed later on) and friction is 0.025 (angle of 1.43°), corresponding to the mean value proposed by Lamb (2006). At 120 km the density of the channel increases, mimicking eclogitization.

The driving boundary conditions are 1) a westward velocity Vr= 3 cm/yr applied from the eastern edge of the model lithosphere, simulating South America plate motion, and 2) a velocity traction Vb = 5 cm/yr inclined at 35°downwards exactly where the oceanic plate intersects the base of the model at 300 km depth (similar to Sobolev & Babeyko, 2005). Lithostatic normal stresses are applied at the base and lateral borders of the model at asthenospheric depths, and along the extremity of the oceanic plate along the left border.

Mechanically, we start from a geometrical configuration of layers of different density, which are compensated only in the vertical direction with the appropriate initial topography. About 1 millions years are needed for the model to build up stresses and deform internally in response to applied assymetric slab-pull and upper plate driving forces. This time-scale is defined by elastic and yield parameters and the loading strain-rate, and can be roughly estimated from 1D Hooke's law: with a maximum yield stress close to 1 GPa, a standard Young's modulous equal to 30 GPa, and ~7 cm/yr of horizontal compression applied over a model length of 1800 km.

3.2.2 – Thermal structure

Thermally, we proceed similarly as in the mechanical approach, in the sense that we presume of initial temperatures close to steady state, that will not evolve significantly during the 2 Myr of the model duration: heat conduction, radioactive heating and shear heating, as well as convective heat transport are all directly limited by the short duration of the run. This short 2 Myr time scale also allows us to neglect evolving phase transformations (eclogitization or serpentinization of the oceanic crust), partial melting, or thermo-chemical effects. The initial thermal structure is thus based on previous estimates by Springer (1999) and Tassara et al. (2006). We first calculate oceanic and continental geotherms as a function of their thermal age (Parsons & Sclater, 1977; Turcotte & Schubert, 1982; Burov & Diament, 1995). We choose an age of 60 Myrs for the oceanic lithosphere, in order to deal with a lithosphere, only slightly but reasonably colder than the unsatisfying "theoretical" 50 Mrs-old age. We thus have surface values of 60 mW/m^2, still greater than the measured 30-40mW/m^2. Implications will be discussed later on. For continental temperatures, we define the thermal depth of the continental plate at 180 km (Tassara et al., 2006), standard radiogenic crustal heating (see table 3), and insert a gaussian shape thermal anomaly initiating from the interplate contact, extending below the Altiplano thickened crust to the Subandean area, that superimposes on Tassara et al. (2006) estimation of the lithosphere-asthenosphere boundary. Tassara et al. (2006) obtained a lithosphere-astenosphere boundary (isotherm 1350°C) moving up to 60 km depth below the Western Cordillera and Altiplano, descending down to 160-180 km depth further East (Figure 5). At the interplate contact, Springer (1999) used a heating shear stress of 15 Mpa, whereas Lamb (2006) employs 10 MPa, from seismic coupling arguments: we insert an interface shear heating stress of 10 MPa.

In fact, we will not follow here the standard approach for thermal modelling of subduction zones, in which a kinematically prescribed slab drives a dynamic corner-flow in the wedge under a stationary overriding plate (e. g. Peacock & Wang 1999; van Keken et al., 2002; Kelemen et al., 2003; Conder, 2005; Kneller et al., 2005, 2007; Abers et al., 2006). These thermal models use an Eulerian method that resolves the temperature equation for a steady state that is reached over several tens of millions of years (ideally 100 Myrs), and allows to study the thermal influence of viscous mantle corner flow on the surrounding plates. Our approach here differs since we only aim at reproducing 2 Ma of thermo-mechanical dynamics, and therefore assume that the thermal state at the onset of the run is equivalent (e.g. does not change significantly) to that at the end of the run: this is a simplified hypothesis, that limits the development of significant mantle corner flow. We will discuss this limitation later on in the light of our results. On the other hand, the advantage of our approach compared to standard thermal models of mantle wedge corner flow, is that we do not fix the position or motion of plates in the subduction zone area during the run, thus we do not need to define special wedge boundary conditions (e.g. Conder 2005; Van Keken et al., 2002), such as a progressive transition between the fixed part and the subducting part of the oceanic plate. Here in our models, no condition other than the initial temperature is applied, since the 10 km thick channel interface, like all other layers, is self-consistently defined with a temperature-dependent brittle-ductile behaviour, located in between both deformable oceanic and continental plates. The approach is thus resolutely different.

3.2.3-Mechanical behaviour of the Reference model

Elements of the model progressively load and deform as they are submitted to the gravity force and the kinematic boundary conditions. They reach a stress threshold that depends on their rheological properties: warm zones deform ductilely, while cold zones deform brittlely. We will here mainly describe deep stresses and temperatures in order to connect them with Pressure-Temperature (PT) petrological inferences from our tomography data. Stress and strain patterns in the continental crust will be only briefly described here, as it is not the aim of this paper to discuss this part of the modeling study, but will be done in another paper.

- In the oceanic lithosphere (green domain in Figures 5 and 6c), flexural stresses develop due to its bended geometry. Before the trench at X~-50 km, brittle shear zones develop at the surface, extending down to several tens of kms into the oceanic mantle (Figure 6b). These outer-rise faults are compatible with previous observations of deep outer-rise events along the Chilean margin (Clouard et al., 2007). As the oceanic lithosphere dips under the continent, tensile stresses develop in direction

parallel to the applied slab-pull velocity (Figure 6e), together with high compressional stress on the top portion of the slab down to about 130 km depth (commented in section 3.3).

- In the subduction channel (yellow to light orange zones in figures 5, 6c), shear deformation develops, at relatively low shear stress (Figures 6d). At the surface a trench forms about 8 km deep. The shear stress reaches ~40 MPa down to ~60 km depth (Figure 7a), consistent with previous estimates (e.g. Lamb, 2006, and references therein), and corresponds approximatively to a brittle-ductile transition. Above, deformation occurs dominantly by brittle failure according to the Mohr-Coulomb criterion at constant friction angle (1.43), and corresponding to the seismogenic zone. Below 80km depth, the subduction channel behaves ductile with a low effective viscosity ($<10^{20}$ Pa.s., Figure 7b).
- The continental upper crust (brown, Figures 5, 6c) deforms mostly brittle, and is partly ductile at ~10 km depth in the Bolivian area (X>~550 km, Figure 6b). The lower crust (red, Figure 6c) remains competent and deforms little in the fore-arc and in the cratonic easternmost domain, in contrast to the Altiplano, where weaker rheology and warmer temperatures enable to develop ductile shear deformation. This area below the plateau links deformation from the subducting slab, eastwards to the surface in the Eastern Bolivian weak upper crust (e.g. Sobolev & Babeyko, 2005). This mode of simple shear deformation is consistent with previous propositions such as by Tassara et al. (2005, 2007).
- As a whole, the fore-arc area behaves as a rigid lithospheric-scale wedge, bounded to the east by the Western Cordillera, and extending down to ~110 km depth. This rigid block is cold and composed of strong crust and mantle rheologies, therefore deforms little (Figure 6b, e.g. Tassara et al., 2007). Observed seismicity occurs in the range <400°C for crustal domains and <600°C for mantle domains (Figure 6c). However, stresses are not homogeneous (Figure 6d-e): seismicity occurs first at the high stress contact of the crust with the subduction channel, and then further east in slightly lower deviatoric stress areas. Principal stresses orientations indicate that this seismicity occurs in a down-dip tensional zone at 30-80 km depth (red crosses at X=140-230 km), and where the most compressive stress (blue crosses) rotates from horizontal to vertical at 10-40 km depth (X~220-300 km).
- The continental mantle (blue, Figures 5, 6c) deforms little at temperatures lower than ~600°C, while it deforms ductile at greater temperatures, and with negligible shear stress (power law temperature dependant olivine rheology). East of and along the subduction channel below the fore-arc, cold temperatures induce significant shear stress (around 100 MPa, figure 6d) in the lithospheric mantle down to about 100 km depth. This cold "rigid mantle wedge" (e.g. Honda, 1985), or more recently named the cold nose (Abers et al., 2006) is delimited on top by the base of the fore-arc crust, at its base by the warmer and ductile corner wedge, and to the west by the nearly vertical ~600°C olivine brittle-ductile transition. While recent thermal studies show the high capacity of mantle corner flow in heating the adjacent slab and the overriding plate (e.g.; Billen & Gurnis, 2001; Van Keken et al., 2002; Currie & Hyndman, 2006; Kelemen et al., 2003), coherent with heat flow and geophysical characteristics of several subduction zones, other thermal models also show that the development of a cold fore-arc mantle wedge is favored when the oceanic plate is old and subducts fast, and when a strong coupling is accounted for in between the fixed and descending parts of the oceanic plate (e.g. Kneller et al., 2005; Abers et al., 2006). The data from Northern Chile indicates such characteristics, with Springer's (1999) thermal model indicating a shallowest depth of the asthenospheric wedge located 70 km below the Western Cordillera, and vertically descending isotherms down to about 100 km depth before intersecting with the slab (such verticalisation is also assumed by Abers et al., 2006, for Cascadia). This cold fore-arc mantle remains the strongest layer of the continental lithosphere, and acts as a butress to subduction, thus controlling deformation of the upper plate. It transmits compressional stresses from the upper plate, that apply perpendicular to the subduction zone, into the slab. The stresses that we obtain are in the range of those cited by Kneller et al. (2005, 2007), who explain trench-parallel fast shear-wave splitting directions by the presence of B-type olivine fabric in the fore-arc mantle. Heading East below the high plateau, high temperatures (1350°C at ~60km depth) provide a low viscosity behaviour that may be associated to active mantle corner flow, coherent with magnetotelluric and seismological data. Below the Eastern Cordillera (X~500 km) and eastward, progressive cooling recomposes a rigid, cratonic like behavior down to >150 km depth.

3.3-DSZ Pressure-Temperature conditions inferred from the thermo-mechanical model

We display now the modeled Pressure–Temperature (PT) conditions in the double seismic zone, spread between 80 and 140 km depth along the slab. Figure 7 displays the thermal and stress conditions within the subducting channel crust, and Figure 8 shows Pressure-Temperature conditions within the slab. We superimpose the earthquake locations and the model (Fig. 6) by assuming that at least the top part of the upper plane of earthquakes should be located inside the subducting oceanic crust channel (yellow in figure 5). The uncertainty in this «visual» fit is about 5 km, due to the projection of seismic profiles on the curved in plane geometry of the trench at these latitudes, and to the thermo-mechanical grid size. Whereas it is common to assume that Wadati-Benioff earthquakes delineate the subduction channel, an uncertainty remains on this assumption, see for example a depth dependent increasing decay in Abers et al. (2006), for the Cascades subduction zone. However, note that in this latter study, this correspondenc is preserved in the upper part of the Wadati-Benioff zone.

3.3.1- Upper DSZ plane

Figure 7c plots minimal and maximal temperatures within the subduction channel: whereas maximum temperatures reach 750°C at the top of the subducting crust, they drastically decrease to about 300°C at the bottom base of the subducting crust, which in the model was defined 10 km thick. In between 90 and 130 km depth, minimum temperatures are ~100°C lower than those estimated by Abers et al. (2006) for the, yet shallower, seismic portion of central Cascadia subduction zone, where a younger 38 Ma oceanic lithosphere converges at a speed of 55mm/yr. Maximum temperatures, however are close to 700°C, which is about 100°C less than what Van Keken et al. (2002) obtained for the top of the Honshu slab below the volcanic arc. Considering the equivalent surface heat-flow between both subducting plates in Honshu and Northern Chile, we evaluate that this 100°C difference is linked with the obviously warmer general temperatures of the Honshu upper plate with respect to Northern Chile (see previous sections).

We have here a possible explanation for the distance measured by Abers et al. (2006) in Cascadia, between the earthquakes of the Wadati-Benioff zone and the low seismic velocity zone: the latter could represent the warmest and thus ductile top of the crust, whereas the former could represent the coldest and thus seismically active base of the subducting crust.

In our prior estimates of petrological compositions using Hacker & Abers (2004) procedure, Vp and Vs values of Northern Chile DSZ upper plane were best modeled with water-rich (up to 5.7 wt% H_2O), and mineral assemblages comprising omphacite, lawsonite, amphibole and chlorite (section 2.2.3). Thermo-dynamically calculated mineral equilibria for metabasaltic compositions (i. e., Guiraud et al., 1990; Clarke et al., 1997; Carlson et al., 1999) all indicate that such mineral assemblages only occur at temperatures below 570°C and are typical of blueschist conditions. In addition, the probable persistence of lawsonite in mineral assemblages suggests that temperatures, even at 3.5 GPa (~140 km) do not exceed ~700°C, the temperature at which lawsonite is no longer stable. Thus, independent mineralogical data are consistent with the low temperature conditions of our thermo-mechanically modelled crust. Then, a fluid release associated to progressive breakdown of H_2O-rich phases, such as chlorite and amphibole, appears as the most probable scenario to explain this upper plane seismicity.

3.3.2- Intermediate zone

Our previous petrological estimates for this zone was a partially hydrated harzburgitic oceanic mantle, with however, remaining high Vp values with respect to Vs and Vp/Vs values (section 2.2.4). We note from the present thermo-mechanical models that along the subduction zone, the DSZ seismicity contours and bounds the shape of the inner-slab compressive zone (Figure 8a) from 80 to 130 km depth. The intermediate zone is thus in a compressional state of stress, at approximately at least 400 MPa above lithostatic stress. Such over-lithostatic pressures of several hundreds of MPa tend to increase Vp (Hacker et al., 2003a), thus offering an explanation to the relative high numbers measured in Northern Chile. We may therefore evaluate that this intermediate zone is even less hydrated than previously estimated.

3.3.3-Lower DSZ plane

If the upper plane's seismicity represents indeed the subducting oceanic crust, then the observed lower plane's seismicity falls in the model, on the neutral plane of the subducting mantle located about 20 km below the top of the slab (Figures 8a, 8c). There, pressure becomes lithostatic as it switches from down-dip compression to down-dip tension (Figure 6e, 8c). This neutral plane could form a secondary channel of «relaxed» pressure, into which fluids from lateral areas could migrate: tensile stresses below the neutral plane should help open pores and let light fluids migrate upwards, whereas compressional stresses above the neutral plane should close pores and create a permeability barrrier to fluid ascent. Consequently, free fluids could remain trapped in this neutral plane. Earthquakes may thus be triggered close to and on either side of this neutral plane, due to the presence of freefluids. Within a partially hydrated harzburgitic material (the most probable candidate deduced insection 2.2.5), such a free-fluid phase pore configuration could explain the observed low Vp/Vs ratios, as suggested by many authors (i.e., Nakajima et al., 2001; Takei, 2002; Hacker et al., 2003a).

Seismic events occurring in this lower DSZ plane should therefore not present any dominant compressional or extensional focal mechanism, but will rather occur depending on their position either slightly above or slightly below this neutral fiber. In fact, previous studies worldwide cannot isolate a common trend for the location of compressional or extensional events in the upper and lower plane of DSZs respectively, nor the opposite (cf. review in Peacock, 2001). Our proposition here differs from previous studies that link upper and lower seismic planes to high deviatoric stresses in the down-going crust and mantle (e.g. Wang, 2002), and for which the elastic core is located in between both seismic planes. Here instead, we propose that the plate's stress neutral fiber has not kept a significantly thick elastic core (e.g. Sleep, 1979), but consists of an already fractured area (such as by outer-rise faulting) in which fluids have accumulated and trigger neighbouring seismogenic dehydration reactions.

Note that in Figure 8c, the minimal distance between the subducting channel and the neutral lithostatic stress is closer to 15 km than to 20 km. We think that this is due to our choice of a relatively warm subducting oceanic lithosphere (60 Myr old) with respect to real conditions infered from surface heat-flow values (corresponding to classical 100 Myr old oceanic lithospheres). With a colder lithosphere, this distance increases, as indicated by Brudzinski et al.'s (2007) study and an alternate cold model (section 3.4). Furthermore, if instead we try to associate the upper and lower plane seismicity to the compressional and extensional zones of the subducting lithosphere respectively, then we see that their distance in the model is 25 km (Fig. 8c), which is not satisfying either, and will even increase if a colder oceanic lithosphere was assumed.

In general, our modeled temperatures are about 100°C lower than those predicted for the Honshu lower seismic plane. Petrological interpretations indicate conditions lower than about 500-600°C, while our thermo-mechanical models indicate conditions around 400°C. There are several possible explanations:

1- Temperatures in the Northern Chile subduction zone are anomalously cold: first the Nazca plate has anomalously low surface heat flow (30mW/m^2 instead of the theoretical 70mW/m^2, e.g. Springer & Forster, 1998), then the overriding plate presents geophysical characteristics of a rigid cold fore-arc as opposed to a very weak and warm Altiplano, indicative of an eastward shift of the warming mantle wedge corner flow (e.g. Haberland et al., 2003; Brasse, 2005). Honda (1985) had already suggested that the mantle fore-arc of central South America is probably cooler than that of the Honshu region, possibly associated to the different nature of volcanic rocks in both regions. More recently, Kneller et al. (2007) proposed to explain trench-parallel fast shear-wave splitting directions in the fore-arc mantle of several subduction zones, including Northern Chile, by the presence of B-type olivine fabric, associated to a relatively cold and a high stress environment. Since we used in our models a Nazca plate age of 60 Myr giving surface heat-flow values of 60mW/m^2, we may still be overestimating inner-slab real temperatures.

2- The numerical models carried here have assumed simple thermal properties that are basically diffusing and advecting during a short 2 Ma time: there is no account for thermal expansion, nor for latent heat linked to phase transformations. Certainly the long-lived subduction zone of Chile incorporates

greater complexity than the present models do. Several studies showed that power-law viscous flow in the mantle wedge is capable of heating the plate interface temperatures by about 200°C compared to isoviscous cases (e.g. van Keken et al., 2002; Conder 2005). Although here we use a similar power-law rheology, the short duration of the model (2 Ma) limits the efficiency of convective heat transport. We may thus be underestimating slab interface temperatures. However, Van Keken et al. (2002) also showed that thermal gradients towards the inner-core of the slab may remain high, especially in cases of fast subduction of cold lithosphere, thus preserving its initial cold state to great depths. Consequently, we may be underestimating temperatures at the top of the slab, but not that much inner-slab temperatures.

3.4- Testing various parameters

The reference model of Figure 6 is our preferred model with which we discussed the PT conditions for the DSZ of Northern Chile. But in order to obtain these appropriate PT conditions, we had to tune a number of initial parameters. Figure 9 shows a set of 5 alternate models, which illustrate the effect of varying some parameters with respect to the reference model (Figure 9a, Table 6):

- First, if we take a 100 Ma old subducting oceanic plate (Figure 9b), then the modeled surface heat flow better matches the data from Northern Chile. The 400°C isotherm and the compressional domain on top of the slab extend deeper down to about 180 km, in good correlation with the deeper DSZ of Honshu (plate age of 130 Ma). Our petrological interpretations, which strongly suggest a cold oceanic plate, still agree with this thermal setting.
- Second, if we take warmer conditions in the overriding plate (Figure 9c), the intensity of the compressional zone vanishes. In this model, the continental thermal thickness (*hl*) was decreased to 120 km, and the thermal anomaly was increased. There, the warm fore-arc mantle flows ductilely and cannot transmit that much high stresses from the upper plate into the subducting plate. Other lines of evidence indicate that the fore-arc mantle in Northern Chile is competent, such as thermal studies and gravity modeling (e.g. Honda, 1985; Tassara et al., 2007). Also, it must be competent enough in order to sustain the stresses generated by the extremely thick crust of the Central Andes. In the opposite case, the Altiplano would collapse and present day deformation would concentrate within the fore-arc and high-plateau areas, and this is not observed. Deformation now mainly occurs in the Bolivian fore-land.
- Third, the composition of the subduction channel (Figure 9d) was modified with ductile creep parameters corresponding to plagioclase, replacing wet granite in the reference model. Now, viscosities are greater in the subduction channel, and higher shear stresses develop there (comparison with the reference model in Figure 7a,b). Shear stresses in the subducting channel below about 80 km depth, absorb part of the normal (and thus compressional) stresses acting on one side and the other of the subduction zone, thus reducing the compressional component that is transmitted from the upper plate into the slab.
- Fourth, the radius of curvature of the subduction zone was reduced to 250 km instead of 450 km (Figure 9e). The radius of curvature, *r,* estimated from Wadati-Benioff zones, mostly ranges from 200 to 500 km (e.g. Wang, 2002). While Honshu and Chile have a similar radius of 450-500 km, New Zealand's dipping seismic zone approximates a 300 km arc radius (Reyners et al., 2006). In this model, compression on top of the slab extend to a shallower depth, consistent with shallowing of the plates unbending depth, but is also extends to greater depth, indicating that plate unbending there, has no more role to play. The slab is seen here to act like a vertical wall that « butresses » horizontal compression.
- Fifth, no upper plate convergence was applied (Figure 9f), the right boundary of the model was maintained fixed in the horizontal direction. In addition, the overthickened crust of the Altiplano was removed, in order to inhibit the local lateral compression exerted by gravitational forces. Now, the intensity of compression on top of the slab is much lower, showing that upper plate convergence is indeed important in the development of inner-slab compression.

These alternate models demonstrate that the inner-slab flexural compressional zone does not only depend on the subducting plate age, but also on the regional stress environment. Transmission of

compressional stresses from the upper plate into the subducting plate in turn, depends on lubrification of the subducting channel, thermal and rheological states of the overriding plate, and relative plate convergence.

4- Conclusion

The results of a high resolution tomography of the Nazca plate Double Seismic Zone beneath North Chile, combined with a thermo-mechanical numerical modelling of the subduction zone, provides new insights on the petrological and thermodynamical properties of the oceanic plate and overriding continental fore-arc. The velocity structure of the upper 140 km of the slab has been obtained, taking advantage of the two seismic planes observed at depths 80 to 140 km. The results highlight the specific characteristics of the zones where earthquakes occur. Moreover, the geodynamical setting leading to the observation of the DSZ, as well as its pressure and temperature conditions have been investigated by the thermo-mechanical modeling. In summary:

- the DSZ in Northern Chile is observed between 80 to 140 km depth. Both seismic planes are separated by ~20 km.
- The upper seismic plane, corresponding to oceanic crust, is characterised by intermediate Vp (~7.7 km/s) and low Vp/Vs (1.67). These values suggest that between 80 and 140 km depth, the seismic upper plane is related to fluids releases associated to metamorphic reactions occurring within jadeite-lawsonite blueschists and perhaps, at higher depths (~130 km) under lawsonite-amphibole eclogite conditions.
- Seismicity in the lower plane, lying in the oceanic mantle, yields low Vp (~7.4 km/s) and low Vp/Vs (~1.57). These values are consistent with the common hypothesis of seismic activity associated to water release resulting from brucite, chlorite and antigorite breakdown in dehydration reactions occurring within serpentinized harzburgite (antigorite ≤ 25 vol. %).
- The region in between the two planes, with high Vp (8.5 km/s) and high Vp/Vs (1.9), presents characteristics corresponding to a moderately serpentinized harzburgite (antigorite ≤10 vol. %).
- Our petrological estimates infer general thermal conditions lower than 500°C. This low temperature range in comparison to estimates from other subduction zones, is justified by the extremely anomalous structure of the Nazca plate, which has surface heat-flow values of ~30mW/m^2 compared to its theoretical 70mW/m^2 (considering its 50 Myr age, Springer & Forster, 1998). Furthermore, the fore-arc mantle into which the Nazca plate subducts is also probably cold and only partially serpentinised, as indicated by previously acquired geophysical data such as Qp attenuation, magnetotellurics or shear wave splitting data. This generally cold state of the subduction zone may have significant implications on the kinetics of metamorphic reactions and on the rock structures. Although water saturated, the slab could display offsets between real parageneses and predicted ones estimated from equilibrium thermodynamics petrogenetic grids. This feature, together with the fact that North Chile DSZ most probably contains partially hydrated rock zones, suggests texturally heterogeneous environments in which rock fragments of metastable mineral assemblages (i. e., gabbro, peridotite) persist within metamorphic rocks of higher metamorphic grade (i. e., blueschist, eclogite) or more hydrated rocks (i. e., serpentinite). Global velocity properties of such environments could be strongly affected by this textural heterogeneity, such as Vp values being more sensitive to the water content of a weak matrix and Vs values being more sensitive to rigid nodules.
- Thermo-mechanical models consistent with a cold environment reproduce the deformation and stress patterns of the subduction zone. In agreement with previous studies, deformation propagates from the subduction channel shear-zone, into the Altiplano lower crust and the Subandean zone, whereas the fore-arc area remains rigid and sustains high stresses down into fore-arc mantle. When these thermo-mechanical models are superimposed on the seismic data, the DSZ is predicted to lie within the 350-450°C range that contours an inner-slab compressional zone from 80 to 140 km depth. This cold temperature range is about 100°C lower than predictions from thermal models for other, yet probably warmer subduction zones. Alternate tests show that warmer slab and fore-arc conditions reduce the

extent and intensity of this inner-slab compressional zone.

- From the thermo-mechanical models, lower plane earthquakes are predicted to occur in the neutral fiber plane between down-dip tension and down-dip compression, where we suggest that fluids released from surrounding metamorphic reactions can migrate. We think that tensile stresses below this neutral plane open pores and favor upward migration of free-fluids, whereas compressive stresses above this neutral plane closes pores and creates a permeability barrier able to trap fluids along a thinly sheeted serpentinized layer. This would be consistent with the generally admitted relation between dehydration reactions and seismicity (Nakajima et al., 2001; Takei, 2002; Hacker et al., 2003a). Therefore these lower plane earthquakes are likely to present both down-dip compression and down-dip extension characteristics, precisely because of their location about the neutral plane. In between both seismic planes, the models produce compressional stresses of several hundreds MPa: this should affect seismic velocities, and in particular, reduce the amount of fluids required to explain observed values.
- Numerical tests indicate that the inner-slab compressional zone depends on the following parameters: 1) an older plate yields deeper isotherms and also deeper compressional zone. 2) a weak ductile subduction channel favors inner-slab compression, by facilitating transmission of compressional stresses from the upper plate. 3) A cold structure of the continental fore-arc also favors inner-slab compression, for the same reason. 4) Decreasing subducting plate radius of curvature broadens the inner-slab compression upward and downwards. 5) decreasing upper plate convergence diminishes it. All these results indicate that if indeed DSZ's contours inner-slab compression in general, they cannot only be linked to slab unbending (e.g. see discussion in Abers, 1992), but also to the transmission of compressional stresses from the upper plate into the slab, as had suggested Fujita and Kanamori (1981). In the case of Honshu and New Zealand, both subducting plates are much older than Northern Chile, but display equivalent surface heat fluxes capable to create the appropriate cool environment for segmented compressional stresses to develop. Furthermore, if we apply Brudzinsky et al.'s (2007) rule of thumb of DSZ separations equal to 0.14 km/Myr, a plate age of 50 Myr should give a separation of 7 km. If we use an effective plate age of 100 Myr more consistent with the observed surface heat-flow in Northern Chile, then this separation should be 14 km, still lower than what is actually obtained in this study. Consequently, there must be another factor than plate age alone, that controls the distance between both seismic planes. The previous models indicate that indeed, the compressional state of stress of the upper plate transmits into the subducting plate, and increases the thickness and magnitude of its own compressional state, thus increasing the DSZ separation. Further global studies should help confirm this effect.

Aknowledgements:

C. D. thanks Clifford Thurber for inviting her to attend the workshop on seismic waveform alignment, earthquake location, and seismic tomography, held at the Department of Geology and Geophysics, UW-Madison, from May 17-21, 2004. M.G. thanks Andres Tassara for helping constraining the models for another issue, Jaime Campos for providing office facilities at Univ. de Chile, system administrators Rodrigo Sanchez in Chile and Guillaume Pernot in Toulouse without who the several hundreds of runs couldn't have been done, Mathurin Lebris for his preliminary implementation of passive markers, and Marko Testi for his magical Matlab tricks.

Table 1: Vp, Vs values and Vp/Vs ratios in the Nazca Plate DSZ obtained in this study.

	Vp (km/s)	***Vs (km/s)***	***Vp/Vs***
upper plane	7.7	4.6	~1.67
region in between	8.5	4.5	~1.89
lower plane	7.4	4.7	~1.57

Table 2: Vp, Vs values and Vp/Vs ratios obtained by tomoDD in other DSZ. Honshu 39°N: Zhang et al. (2004), Honshu 37°N: Shelly et al. (2006), New Zealand 41°S: Zhang (2003).

	Region	***Vp (km/s)***	***Vs (km/s)***	***Vp/Vs***
upper plane	Honshu 39°N Honshu 37°N NewZealand 41°S	7.8 – 8.0 8.5 7.5	4.4 – 4.5	1.72 – 1.85 1.82 1.65
region in between	Honshu 39°N Honshu 37°N NewZealand 41°S	8.2 – 8.4 8.5	4.6	1.8 – 1.85 1.9
lower plane	Honshu 39°N Honshu 37°N NewZealand 41°S	7.6 – 7.8 8.0 7.0 – 7.5	4.7 – 4.9	1.6 – 1.7 1.7 1.55

Table 3. Notations and physical values common for all experiments (Turcotte & Schubert, 1982). Bold values are those that were tested and displayed Figure 8.

Parameter	Values and units	Definition
P	Pa, MPa	Stress, pressure
ε	s^{-1}	Strain
μ*	10^{10}-10^{20} Pa s	Effective viscosity
ϕ	1.5-20°	Friction angle (see Table 4)
So	10 MPa	Cohesion
λ , G	30 GPa	Lamé elastic constants (λ = G)
Vx	**3 cm/yr -0**	Horizontal upper plate convergence
Vb	5 cm/yr	Basal slab-pull velocity
r	**250-450 km**	Radius of curvature of oceanic plate
hc	35-55 km	Normal and pre-thickened continental Moho depth
hl	**120-180 km**	Thickness of lithosphere
T, To, Tb	10°-1350°	Temperature, surface, base
Cp	10 J/kg /°C	Specific heat
Δ*T*	9-12°C/km	Initial arc anomaly, with maximum at X=330-530 km
α	3×10^{-5} /°C	Thermal expansivity
k*c*	2.5 -2.9-3.3W/m/°C	Thermal conductivity, crust, mantle, channel
H	$9.\times10^{-10}$ W kg-1	Radiogenic heat production, constant
hr	10 km	Radiogenic heat production exponential decay depth
AC	400 Ma	Thermotectonic age of the continental lithosphere
AO	**60-150 Ma**	Age of the oceanic lithopshere
lc	10 km	Thickness of subduction channel
ke	25, 2000 m^2/yr	Erosional diffusion coef., left & right of the Eastern Cordillera

Table 4: Model parameters: density (ρ), compared to those chosen by Tassara et al. (2006), dominant composition (labels given in Table 5), friction (ϕ), conductivity (k), for models layers. Value in bold was modified for model *8d*.

	Oceanic mantle	*Oceanic Crust*	*Asthenosphere*	*Continental upper crust*	*Continental lower crust*	*Continental mantle*	*Subducting sediments*	*Subduction channel*
ρ	3350	3050	3350	2750	3050	3340	2750	3250-3370
$\rho_{Tassara}$	3260-3500	2980	3310-3450	2700	3100	3240-3320	2980	2980-3550
compos.	*oldry*	*mfgr*	*oldry*	*qz*	*mfgr*	*olwet*	*plg*	***wetgr-plg***
k	3.3	2.9	3.3	2.5	2.5	3.3	2.9	2.9
ϕ	20°	15°	5°	15°	15°	5°	5°	1.5°

Table 5: Dislocation creep parameters (*n* power exponent, *A* material constant, *Q* activation energy), after references provided in Ranalli, 1995.

	Dry Olivine *oldry*	Wet Olivine *olwet*	Mafic granulite *mfgr*	Plagioclase *Plg*	Quartz *qz*	Wet Granite *wetgr*
n	3	2.5	4.2	3.2	2	1.9
A ($MPa^{-n/s}$)	7.e4	3.e4	1.4e4	3.3e-4	1.e-3	2.e-4
Q ($Jmol^{-1}$)	5.2e5	4.44e5	4.45e5	2.38e5	1.67e5	1.37e5

Table 6: Models tested parameters. Specific variation for each model is shown in bold (See Figure 8, and Tables 3, 4, 5 for more details).

	Oceanic plate age	Continental temperature	Creep parameters for channel	Plate curvature	Upper plate
a) Reference model	**60 Ma**	***hl*=180 km + 9°/km**	**wet granite**	**450 km**	**3cm/yr + prethickened crust**
b) Old oceanic plate	**160 Ma**	*hl*=180 km + 9°/km	wet granite	450 km	3cm/yr + prethickened crust
c) Warm continent	60 Ma	***hl*=120 km + 10°/km**	wet granite	450 km	3cm/yr + prethickened crust
d) High viscosity channel	60 Ma	*hl*=180 km + 9°/km	**plagioclase**	450 km	3cm/yr + prethickened crust
e) Small plate curvature	60 Ma	*hl*=180 km + 9°/km	wet granite	**250 km**	3cm/yr + prethickened crust
f) No upper plate compression	60 Ma	*hl*=180 km + 9°/km	wet granite	450 km	**0cm/yr**

References

Abers, G.A. (1992), Relationship between shallow-and intermediate depth seismicity in the Eastern Aleutian subduction zone, *Geophys. Res. Lett.*, *19*, 2019-2022.

Abers, G.A., P. van Keken, E.A. Kneller, A. Ferris, and J. Stachnik (2006), The thermal structure of subduction zones constrained by seismic imaging: Implications for slab dehydration and wedge flow, *Earth Planet. Sci. Lett., 241*, 387-397.

Beck, S. L., and G. Zandt (2002), The nature of orogenic crust in the central Andes, *J. Geophys. Res.*, *107*(B10), 2230, doi:10.1029/2000JB000124.

Benn, K., A. Nicolas, and I. Reuber (1988), Mantle-crust transition zone and origin of wehrlitic magmas : evidence from the Oman Ophiolite. *Tectonophysics*, *151*, 75-85.

Billen M. I., and M. Gurnis (2001), A low viscosity wedge in subduction zones, *Earth Planet. Sci. Lett., 193*, 227-236.

Brasse H., P. Lezaeta, V. Rath, K. Schwalenberg, W. Soyer, and V. Haak (2002), The Bolivian Altiplano conductivity anomaly, *J. Geophys. Res*., 107(B5), doi 10.1029/2001JB000391.

Brasse, H. (2005), The mantle wedge in the Bolivian orocline in the view of deep electromagnetic soundings. Extended Abstract, 6th International Symposium on Andean Geodynamics, Barcelona.

Brudzinski, M.R., C.H. Thurber, B. R. Hacker, and R.E. Engdahl (2007), Global Prevalence of Double Benioff Zones, *Sciences, 316,* 1472-1474.

Burov, E.B., and M. Diament (1995), The effective elastic thickness of continental lithosphere: what does it really mean?, *J. Geophys. Res*., *100*, 3905–3927.

Burov, E.B., and A. Poliakov (2001), Erosion and rheology controls on syn- and post-rift evolution: verifying old and new ideas using a fully coupled numerical model, *J. Geophys. Res., 106*, 16461–16481.

Burov E.B., C. Jaupart, and L. Guillou-Frottier (2003), Ascent and emplacement of magma reservoirs in brittle-ductile upper crust, *J. Geophys. Res., 108*, 2177, doi:10.1029/2002JB001904.

Cande, S.C., and W.E. Haxby (1991), Eocene propagating rifts in the southwest Pacific and their conjugate features on the Nazca plate, *J. Geophys. Res.*, *96*, 19609-19622.

Carson, C.J., R. Powell, and G.L. Clarke (1999), Calculated mineral equilibria for eclogites in CaO-Na_2O-FeO-MgO-Al_2O_3-SiO_2-H_2O: application to the Pouébo Terrane, Pam Peninsula, New Caledonia, *J. metamorphic Geol.*, *17*, 9-24.

Ceuleneer, G., A. Nicolas, and F. Boudier (1988), Mantle flow patterns at an oceanic spreading centre : the Oman peridotites record,*Tectonophysics*, *151*, 1-26.

Christensen, U. (1996), Poisson's ratio and crustal seismology, *J. Geophys. Res*., *101*, 3139-3156.

Clarke, G.L., J.C. Aitchison, and D. Cluzel (1997), Eclogites and Blueschists of the Pam Peninsula, NE New Caledonia: a reappraisal, *J. Petrol.*, *38*, 843-876.

Clouard, V., J. Campos, A. Lemoine, A. Perez, and E. Kausel (2007), Outer rise stress changes related to the subduction of the Juan Fernandez Ridge, central Chile, *J. Geophys. Res*., *112*, B05305, doi:10.1029/2005JB003999.

Coleman, R. G., and T.E. Keith (1971), A chemical study of serpentinisation, Burro Mountain, California, *J. of Petrol.*, *12*, 311-328.

Comte, D., and G. Suarez (1994), An Inverted Double Seismic Zone in Chile: Evidence of Phase Transformation in the Subducted Slab, *Science*, *263*, 212-215.

Comte, D., L. Dorbath, M. Pardo, T. Monfret, H. Haessler, L. Rivera, M. Frogneux, B. Glass, and C. Meneses (1999), A Double-Layered Seismic Zone in Arica, Northern Chile, *Geophys. Res. Lett.*, *26*, 1965-1968.

Comte, D., J. Battaglia, C. Thurber, H. ZhangL. Dorbath, and B. Glass (2004), High-resolution Subducting Slab Structure Beneath Northern Chile Using the Double-Difference Method, *Eos. Trans. AGU, 85 (47),* Fall Meet. Suppl.

Conder, J.A. (2005), A case for hot slab surface temperatures in numerical viscous flow models of subduction zones with improved fault zone parameterization, *Phys. Earth Planet. Int. 149,* 155–164.

Cundall, P., and M. Board (1988), A microcomputer program for modeling large-strain plasticity problems, *Numer. Methods Geomech*., *6*, 2101–2108.

Currie C.A., and R.D. Hyndman (2006), The thermal structure of subduction zone back arcs, *J. Geophys. Res*., *111,* B08404, doi:10.1029/2005JB004024.

DeMets, C., R.G. Gordon, D.F. Argus, and S. Stein (1990), Current plate motions, *Geophys. J. Int.*, *101*, 425-478.

Engdahl, E. R., and C.H. Scholz (1977), A double Benioff zone beneath the central Aleutians: An unbending of the lithosphere, *Geophys. Res. Lett.*, *4*, 473–476.

Evans, B.W. (2004), The serpentinite multisystem revisited: chrysotile is metastable, *Intern. Geol. Rev.*, *46*, 479-506.

Fujita, K., and H. Kanamori (1981), Double seismic zones and stresses of intermediate depth earthquakes, *Geophys. J. R. astr. Soc.*, *66*, 131-156.

Gerbault M., S. Henrys, and F. Davey (2003), Numerical models of lithospheric deformation forming the Southern Alps of New Zealand, *J. Geophys. Res., 108*(B7), 2341, doi:10.1029/2002JB001880.

Graeber, M., and G. Asch (1999), Three-dimensional models of P wave velocity and P-to-S velocity ratio in the southern central Andes by simultaneous inversion of local earthquake data, *J. Geophys. Res.*, *104(*B9), 20,237-20,256.

Guiraud, M., T. Holland, and R. Powell (1990), Calculated mineral equilibria in the greenschist-blueschisteclogite facies in Na_2O-FeO-MgO-Al_2O_3-SiO_2-H_2O. Methods, results and geological applications, *Contrib. Mineral. Petrol., 104*, 85-98.

Haberland, C., A. Rietbrock, B. Schurr, and H. Brasse (2003), Coincident anomalies of seismic attenuation and electrical resistivity beneath the southern Bolivian Altiplano plateau, *Geophys. Res. Lett.*, 30(18), 1923, doi:10.1029/2003GL017492.

Hacker, B.R., and G.A. Abers (2004), Subduction factory 3: an Excel worksheet and macro for calculating the densities,

seismic wave speeds, and H_2O contents of minerals and rocks at pressure and temperature. *Geochem., Geophys. Geosyst.*, *5*, 1-7.

Hacker, B.R., G.A. Abers, and S.M. Peacock (2003a), Subduction factory 1.Theoretical mineralogies, densities, seismic wave speeds, and H_2O contents, *J. Geophys. Res*., *108*(B1), 2029, doi:10.1029/2001JB001127.

Hacker, B. R., S. M. Peacock, G. A. Abers, and S. D. Holloway (2003b), Subduction factory, 2, Are intermediate-depth earthquakes in subducting slabs linked to metamorphic dehydration reactions?, *J. Geophys. Res*., *108*(B1), 2030, doi: 10.1029/2001JB001129.

Hamza, V.M. and M. Muñoz (1996), Heat flow map of South America, *Geothermics, 25*, 6, 599, doi:10.1016/S0375-6505(96)00025-9.

Hasegawa, A., N. Umino, and A. Takagi (1978), Double-planed deep seismic zone and upper mantle structure in the northeastern Japan arc, *Geophys. J. R. astr. Soc.*, *54*, 281-296.

Honda, S. (1985), Thermal structure beneath Tohoku, Northeast Japan- a case study for understanding the detailed thermal structure of the subduction zone, *Tectonophysics, 112*, 69-102**.**

Hyndman, R.D. and S.M. Peacock (2003), Serpentinization of forearc mantle, *Earth Planet. Sci. Lett., 212,* 417- 432.

Isacks, B. L., and M. Barazangi (1977), Geometry of Benioff zones: Lateral segmentation and downwards bending of the subducted lithosphere, in *Island Arcs, Deep Sea Trenches, and Back-arc Basins*, edited by M. Talwani and W. C. Pitman, III, pp. 99–114, AGU, Washington.

Ji S., and Z. Wang (1999), Elastic properties of forsterite-enstatite composites up to 3.0 GPa., *J. Geodyn.*, *28*, 147–174.

Jung, H., H.W. Green II, and L.F. Dobrzhinetskaya (2004), Intermediate-depth earthquake faulting by dehydration embrittlement with negative volume change, *Nature*, *428*, 545, doi:10.1038/nature02412.

van Keken, P.E., B. Kiefer, S.M. Peacock (2002), High-resolution models of subduction zones: implications for mineral dehydration reactions and the transport of water into the deep mantle, *Geochem. Geophys. Geosyst.*, *3*, doi:10.1029/ 2001DC000256.

Kelemen, P.B., J.L. Rilling, E.M. Parmentier, L. Mehl and B.R. Hacker (2003), Thermal structure due to solid-state flow in the mantle wedge beneath arcs, in: *Inside the SubductionFactory, AGU Geophys. Monogr*. *138*, edited by J.M. Eiler, pp. 293-311, AGU, Washington.

Kirby, S. H., E. R. Engdahl, and R. Denlinger (1996), Intermediate-depth intraslab earthquakes and arc volcanism as physical expressions of crustal and uppermost mantle metamorphism in subducting slabs, in *Subduction: Top to Bottom*, *AGU Monograph 96*, edited by G. E. Bebout et al., pp. 195–214, AGU, Washington.

Kneller, E. A., P. E. van Keken, I. Katayama, S. Karato, and J. Park (2005), B-type olivine fabric in the mantle wedge: Insights from high-resolution non-Newtonian subduction zone models, *Earth Planet. Sci. Lett., 237*, 781-797.

Kneller, E. A., P. E. van Keken, I. Katayama, and S. Karato (2007), Stress, strain, and B-type olivine fabric in the fore-arc mantle: Sensitivity tests using high-resolution steady-state subduction zone models, *J. Geophys. Res.*, *112*, B04406, doi:10.1029/2006JB004544.

Lamb, S.H., P. Davis (2003), Cenozoic climate change as a possible cause for the rise of the Andes, *Nature*, *425*, 792–797.

Lamb, S. (2006), Shear stresses on megathrusts: implications for mountain building behind subduction zones, *J. Geophys. Res., 111*, B07401, doi:10.1029/2005JB003916,

Lavier L., W. Buck, and A. Poliakov (1999), Self-consistent rolling-hinge model for the evolution of large-onset low-angle normal faults, *Geology, 27* , 1127–1130.

Le Pourhiet, L., E. Burov, and I. Moretti (2004), Rifting through a stack of inhomogeneous thrusts (the dipping pie concept), *Tectonics*, *23* (4), 1-14.

Lucassen, F., R. Becchio, R. Harmon, S. Kasemann, G. Franz, R. Trumbull, R.L. Romer, and P. Dulski (2001), Composition and density model of the continental crust in an active continental margin – the Central Andes between 18° and 27° S. *Tectomophys., 341,* 195-223.

Nakajima, J., T. Matsuzawa, A. Hasegawa, and D. Zhao (2001), Three-dimensional structure of Vp, Vs, and Vp/Vs beneath northeastern Japan: Implications for arc mgmatism and fluids, *J. Geophys. Res.*, *106*(B10), 21,843-21,858, doi:10.1029/2000JB000008.

Parsons, B., and J.G. Sclater (1977), An analysis of the variation of ocean floor bathymetry and heat flow with age, *J. Geophys. Res.*, *82*, 803-827.

Peacock, S.M. and K. Wang (1999), Seismic Consequences of Warm Versus Cool Subduction Metamorphism: Examples from Southwest and Northeast Japan, *Science, 286,* 937- 939.

Peacock, S.M. (2001), Are the lower planes of double seismic zones caused by serpentinite dehydratation in subducting oceanic mantle?, *Geology*, *29*, 299-302.

Perrillat, J.P., I. Daniel, K.T. Koga, B. Reynard, H. Cardon, and W.A. Crichton (2005), Kinetics of antigorite dehydration: a real-time X-ray diffraction study, *Earth Planet. Sci. Lett.*, *236*, 899-913.

Poliakov A., and Y. Podladchikov (1992), Diapirism and topography, *Geophys. J. Int., 109,* 553-564.

Poliakov A., H.J. Hermann, Y. Podladchikov, and S. Roux (1994), Fractal plastic shear bands, *Fractals 2,* 567-581.

Prince, R. A., and L.D. Kulm (1975), Crustal rupture and the initiation of imbricate thrusting in the Peru-Chile Trench. *Geol. Soc. Amer. Bull.*, *86*, 1639-1653.

Ranalli, G. (1995), *Rheology of the Earth*, Chapman and Hall, London.

Reyners M., D. Eberhart-Phillips, G. Stuart, and Y. Nishimura (2006), Imaging subduction from the trench to 300 km depth beneath the central North Island, New Zealand, with Vp and Vp/Vs, *Geophys. J. Int., 165*, 565–583, doi: 10.1111/j.1365-246X.2006.02897.

Rietbrock A., and F. Waldhauser (2004), A narrowky spaced double-seismic zone in the subducting Nazca plate, *Geophys. Res. Lett., 31*, doi:10.129/2004GL019610.

Roperch P., T. Sempere, O. Macedo, C. Arriagada, M. Fornari, C. Tapia, M. Garcia, and C. Laj (2006), Counterclockwise rotation of late Eocene-Oligocene forearc deposits in southern Peru and its significance for oroclinal bending in the Central Andes, *Tectonics*, *25*, TC3010, doi:10.1029/2005TC001882.

Seno, T., and Y. Yamanaka (1996), Double seismic zones, compressional deep outer-rise events, and superplumes, in *Subduction: Top to Bottom*, *AGU Monograph 96*, edited by G. E. Bebout et al., pp. 347–355, AGU, Washington.

Schilling, F.R.,·R.B. Trumbull, H. Brasse,· C. Haberland, G. Asch, D. Bruhn. K. Mai, V. Haak, P. Giese, M. Muñoz, J. Ramelow, R. Rietbrock, E. Ricaldi, and T. Vietor (2006), Partial Melting in the Central Andean Crust: a Review of Geophysical, Petrophysical, and Petrologic Evidence, in *The Andes,* edited by Oncken et al., pp 459-474, Frontiers in Earth Sciences, Springer, Berlin.

Schurr, B., and A. Rietbrock (2004), Deep seismic structure of the Ata-cama basin, Northern Chile, *Geophys. Res. Lett.*,*31*, : doi 10.1029/ 2004GL019796.

Shelly, D.R., G.C. Beroza, H. Zhang, C.H., Thurber, and S. Ide (2006), High-resolution subduction zone seismicity and velocity structure beneath Ibaraki Prefecture, Japa*n, J. Geophys. Res.*, *111*, B06311, doi:10.1029/2005JB004081.

Sleep, N. H. (1979), The double seismic zone in downgoing slabs and the viscosity of the mesosphere, *J. Geophys. Res., 84*, 4565-4571.

Sobolev, S.V., and A.Y. Babeyko (2005), What drives orogeny in the Andes? *Geology, 33*(8), 617–620.

Sobolev, S.V., and A.Y. Babeyko (2006), Modeling subduction of the continental crust at the Andean type convergent margin, *Geochim. Cosmochim. Acta, 70,* 18, A601, doi:10.116/j.gca.2006.06.1116.

Springer, M., A. Forster (1998), Heat-flow density across the Central Andean subduction zone, *Tectonophysics*, 291,123-139.

Springer, M. (1999), Interpretation of heat-flow density in the Central Andes, *Tectonophysics*, *306*, 377–395.

Syracuse, E.M., and G.A. Abers (2006), Global compilation of variations in slab depth beneath arc volcanoes and implications, *Geochem. Geophys. Geosyst., 7,* Q05017 doi:10.1029/2005GC001045.

Takazawa, E., T. Okayasu, and K. Sahoh (2003), Geochemistry and origin of the basal lherzolites from the northern Oman Ophiolite (northern Fizh Block), *Geochem. Geophys. Geosyst.*, *4*, 1-31.

Takei, Y (2000), Acoustic properties of partially molten media studied on a simple binary system with a controllable dihedral angle, *J. Geophys. Res.*, *105*, 16,665-16,682.

Takei, Y (2002), Effect of pore geometry on Vp/Vs: From equilibrium geometry to crack, *J. Geophys. Res*., *107*(B2), 2043, doi:10.1029/2001JB000522.

Tassara, A., (2005), Interaction between the Nazca and South American plates and formation of the Altiplano–Puna plateau: Review of a flexural analysis along the Andean margin (15°–34°S), *Tectonophysics, 399,* 39–57.

Tassara, A. (2006), Factors controlling the crustal density structure underneath active continental margins with implications for their evolution, *Geochem. Geophys. Geosyst.*, *7*, Q01001, doi:10.1029/2005GC001040.

Tassara, A., H.-J. Götze, S. Schmidt, and R. Hackney (2006), Three-dimensional density model of the Nazca plate and the Andean continental margin, *J. Geophys. Res., 111,* B09404, doi: 10.1029/2005JB003976.

Tassara A., C. Swain, R. Hackney, and J. Kirby (2007), Elastic thickness structure of South America estimated using wavelets and satellite-derived gravity data, *Earth Planet. Sci. Letters*, *253*, 17–36.

Thurber, C.H. (1983), Earthquake locations and three-dimensional crustal structure in the Coyote Lake area, central California, *J. Geophys. Res*., *88*, 8226-8236.

Thurber, C.H. (1993), Local earthquake tomography: velocities and Vp/Vs-theory, in *Seismic Tomography: Theory and Practice*, edited by Iyer, H.M. & Hirahara, pp. 563- 583, K., Chapman and Hall, London.

Turcotte, D., and G. Schubert (1982), *Geodynamics: applications of continuum physics to geological problems,* John, New York.

Waldhauser, F. (2001), hypoDD: A computer program to compute double-difference hypocenter locations, *Open File Rep. 01-113*, 25pp., U.S. Geol. Surv.

Wang, K. (2002), Unbending combined with dehydration embrittlement as a cause for double and triple seismic zones, *Geophys. Res. Lett.*, *29*, doi:10.1029/2002GL015441.

Watanabe, T. (1993), Effects of water and melt on seismic velocities and their application to characterization of seismic reflectors, *Geophys. Res. Lett.*, *20*, 2933-2936.

Yamasaki, T., and T. Seno (2003), Double seismic zone and dehydratation embrittlement of the subducting slab, *J. Geophys. Res.*, *108*, B4, 2212, doi:10.1029/2003JB001918.

Yamato, P., P. Agard, E. Burov, L. Le Pourhiet, L. Jolivet, and C. Tiberi (2007), Burial and exhumation in a subduction wedge: Mutual constraints from thermomechanical modeling and natural P-T-t data (Schistes Lustrés, western Alps), *J. Geophys. Res.*, doi:10.1029/2006JB004441, in press.

Zhang, H. (2003), Double difference seismic tomography method ans its application, PHD thesis, 189pp, Univ. Wisconsin-Madison,.

Zhang, H., and C.H. Thurber (2003), Double-Difference Tomography: The Method and its Application to the Hayward Fault, California, *Bul. Seism. Soc. Am*., *93(*5), 1875-1889.

Zhang, H., C.H. Thurber, D. Shelly, S. Ide, G.C. Beroza,and A. Hasegawa (2004), High-resolution subducting-slab structure beneath Northern Honshu, Japan, revealed by double-difference tomography, *Geology*, *32(*4), 361-364.

Zhao, D., A. Hasegawa, and S. Horiuchi (1992), Tomographic imaging of P and S wave velocity structure beneath northeastern Japan, *J. Geophys. Res., 97,* 19,909-19,928.

Figure Captions

Figure 1: Epicenters of the 2052 events used in the tomography, the darker, the deeper. Red and blue triangles are stations. In gray, the inversion grid used for the inversion. The black cross is the origin of the model (18°S, 69°W). Thin red lines locate the three profiles P1, P2 and P3 presented Figure 3, and the thick red line, the cross section location shown in Figure 4.
Insert: Central Andes tectonic setting between 17° and 20.5°S, from Tassara (2005). cc: Coastal Cordillera, id: Intermediate Depression, dc: Domeyko Cordillera, wc: Western Cordillera, ap: Altiplano. Black vector: Nazca plate absolute motion.

Figure 2: Initial layered model (blue) and final Vp model (red) obtained by 1D inversion.

Figure 3: Cross section through the Vp and Vs values along the 3 profiles shown on Figure 1. Plotted earthquakes are within a 20 km wide section. At depths 80–140 km, the double seismic zone is well defined. Both seismic planes are 5 to 10 km thick with a separation of 20 km. Structures above the white line, where derivative weight sum for each node is more than 10, is meaningful.

Figure 4: Zoom on the velocity structure of the DSZ: cross sections through the Vp and Vs values in the central part of profile P2 (Y=-60 km).

Figure 5: Initial conditions for the thermo-mecanical model: each colored layer has specific rheological density and thermal properties (see Tables 3,4,5). Isotherms 400, 600, 1000, 1300°C are contoured. Asthenospheric and continental mantle in blue, crustal layers in red to brown, oceanic plate in green (crust is in orange), subducting channel in yellow and light orange). Initial topography is evaluated from initial isostatic equilibrium. Boundary conditions are lithostatic compensation on the sides and at the base of the model (narrow black arrows), except at the base of the slab and along the right edge of the continental lithosphere, where velocities of respectively 5cm/yr (slab-pull) and 3cm/yr (upper plate convergence) are applied (bold arrows).

Figure 6: Reference model,with superimposed seismicity. From top to Bottom: **a)** modeled topography in blue, erosion rate in green, and real topography at 18.5°S in black. **b)** Shear strain rate and velocity vectors, indicating in red areas of greater shear deformation, either brittle or ductile (note the outer-rises). **c)** Rheological layers and isotherms: note the 400°C isotherm. **d)** Deviatoric shear stress indicating in red areas of stress greater than 250 MPa, in the slab, in the crust. Note some stress in the deep portions of the fore-arc. **e)** Crosses of the principal stresses, zoomed at the subduction zone, showing down-dip compression above down-dip tension, and rotating and complexe stresses in the fore-arc.

Figure 7: Thermo-mechanical properties of the subduction channel for reference model (red) and model with prescribed higher viscosity in the subduction channel (blue, model *d* figure 8). **a)** deviatoric shear stress, indicating for the reference model a maximum at ~30 km depth of 40 MPa, reducing to nearly 0 below ~80 km depth. **b)** effective viscosity, which becomes lower than 10^20 Pa.s. in the reference model, to the difference of model *d.* **c)** Minimum (dashed lines) and maximum (plain lines) temperatures. Note that the great increase around ~90km depth corresonds to the detachement and elevation of light oceanic crust material throughout the continental mantle (see yellow bubble in figure 6c).

Figure 8 : Pressure-Temperature conditions obtained for the suggested lower seismic plane, located at the depth of the neutral plane in the subducting slab: **a)** Background colors show pressure, with subtraction of the lithostatic component (compression is negative and blue). **b)** Pressure-temperature paths: green markers (dots) and green line (mean value) show the neutral plane within the slab (labeled Plithos), indicating temperatures of 320~380°C at lithostatic pressure of 2.5-5 GPa. Pressure and temperature paths are also shown in blue and red, for areas above and below this neutral plane, which are at an overpressure and underpressure of 200 Mpa respectively, corresponding to the compressive stress (labeled Plithos+200MPa) and tensile stress (Plithos-200MPa) of Figure 8a. See appendix 4 for numerical sampling details. **c)**

Vertical sections of pressure (tension > 0 here, and the lithostatic component is subtracted) throughout the fore-arc, locating from left to right the neutral plane at depths 80, 100, 120 and 140 km (green circles). Note the ~15 km distance of this neutral plane with the subducting channel crust above, whereas the distance between maximum compression and maximum tension is greater than 25 km. Note the variable stress state, including tension, in the fore-arc mantle and in the channel area (pink ellipses).

Figure 9: Reference model and 5 alternate models, showing pressure (the opposite of compression which is negative here, in blue) minus the lithostatic component, and isotherms along the slab. **a)** Reference model. **b)** Cold 150 Ma old oceanic plate, 300°C isotherm exceeds 160 km depth and inner-slab compression is high, broadens and deepens. **c)** Warm continent, 400°C isotherm narrows and compression shallows to 100 km depth. **d)** High viscosity of the deep subduction channel, tension propagates into the fore-arc and inner-slab compression vanishes at 90 km depth. **e)** Small slab curvature of 250 km, isotherms deepen and inner-slab compression elongates from ~30 to 160 km depth. **f)** no applied upper plate convergence and no pre-thickened crust, blurry compression appears from 80-120 km depth.

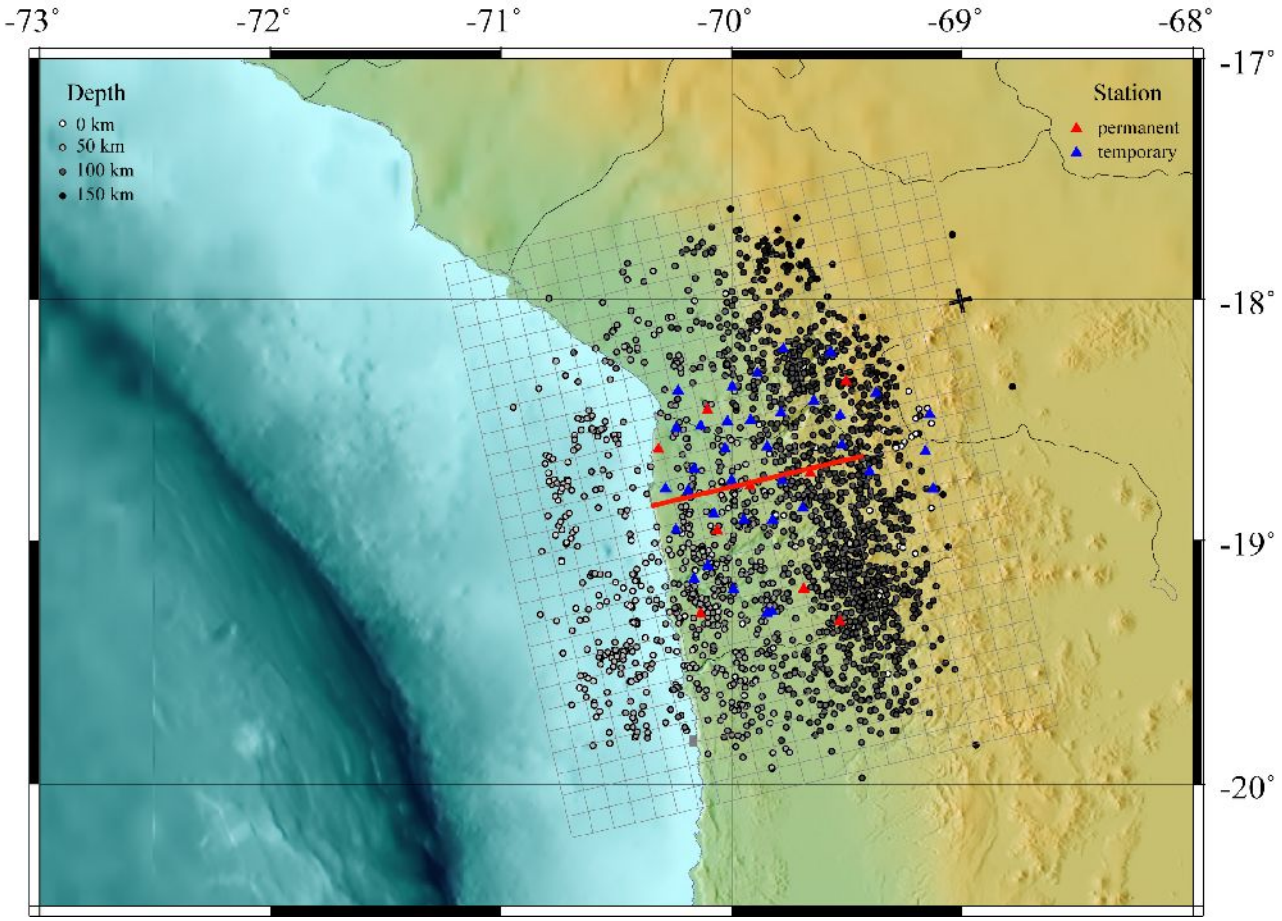
-73°
-72°
-71°
-70°
-69°
-68°
-17°
-18°
-19°
-20°
Depth
0 km
50 km
100 km
150 km
Station
permanent
temporary

Figure 1

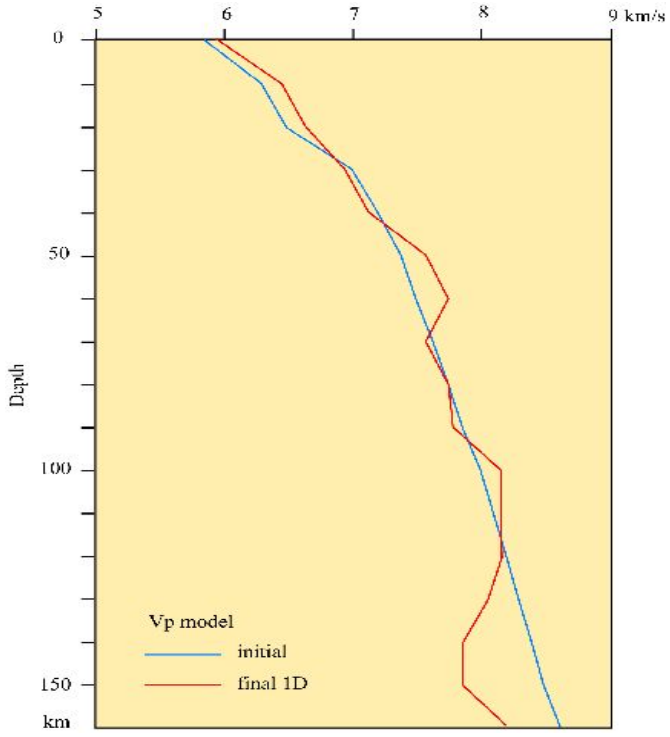

Figure 2

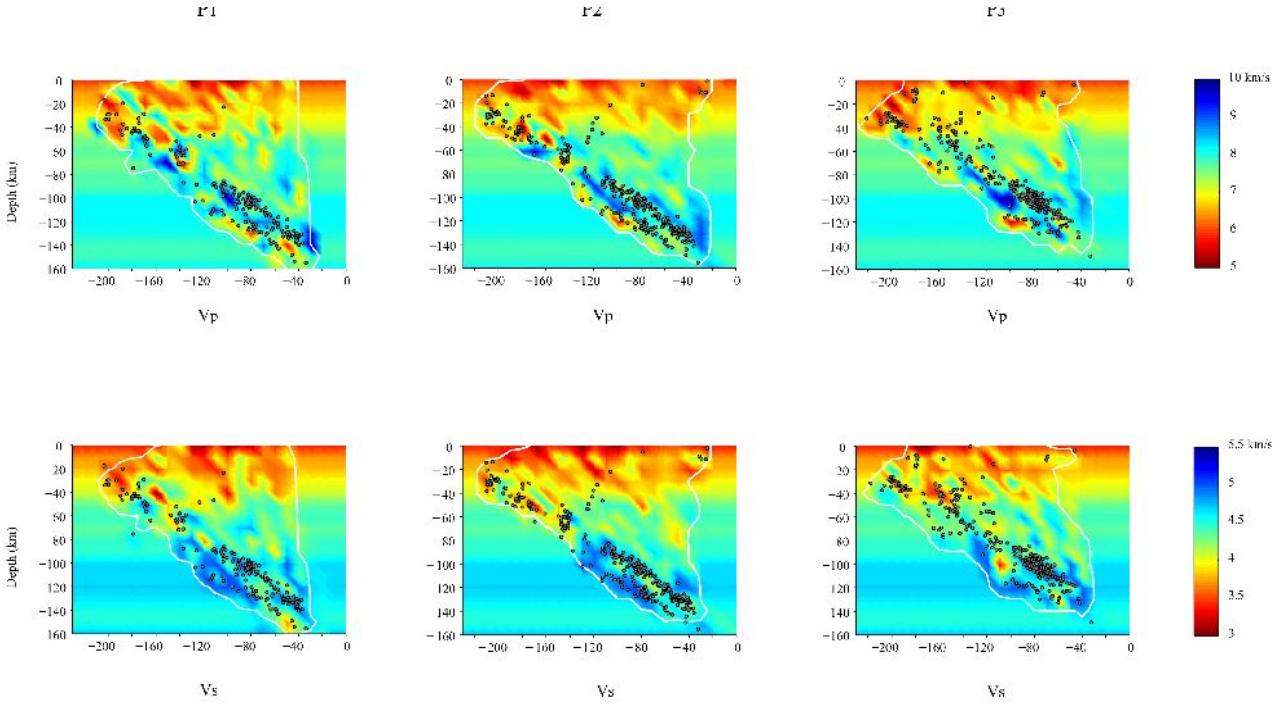

Figure 3

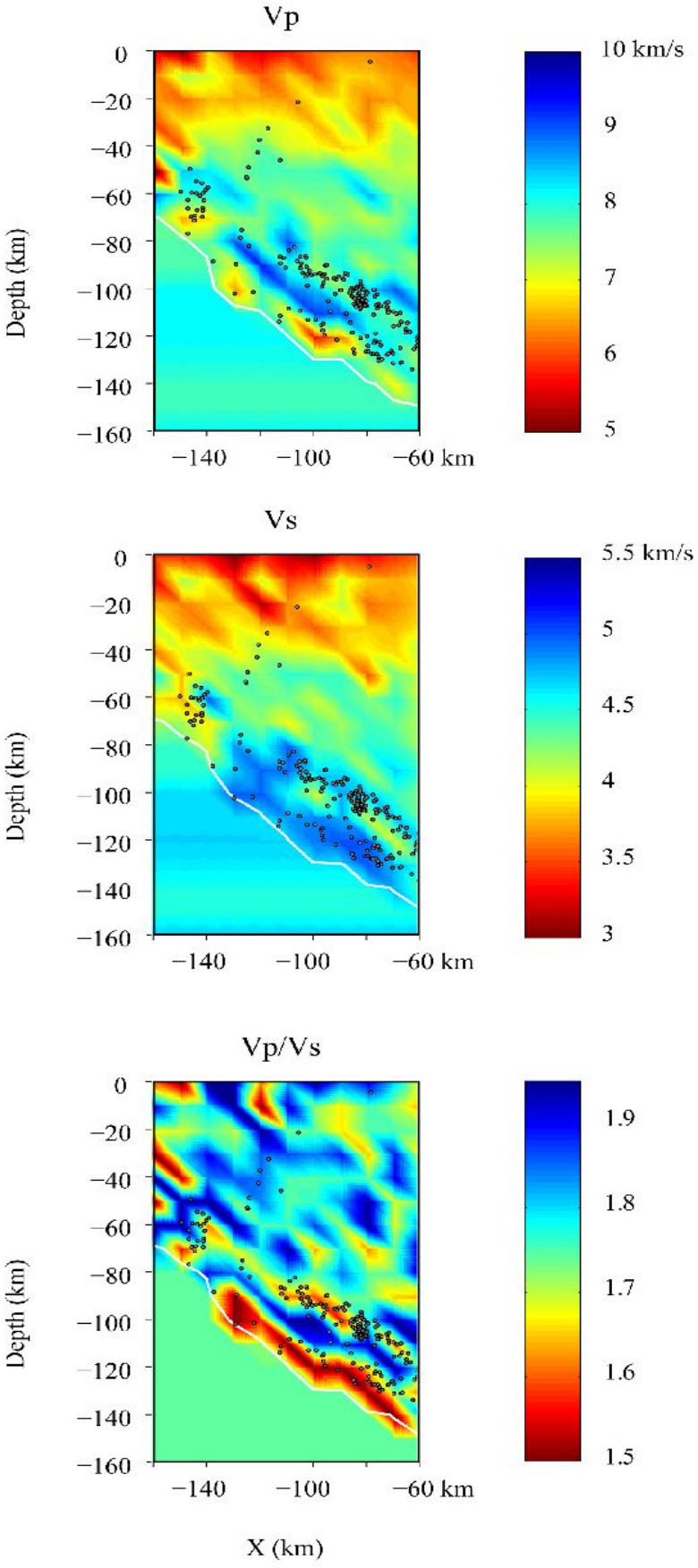
Vp
0
−20
−40
−60
−80
−100
−120
−140
−160
Depth (km)
−140
−100
−60 km
10 km/s
9
8
7
6
5
Vs
0
−20
−40
−60
−80
−100
−120
−140
−160
Depth (km)
−140
−100
−60 km
5.5 km/s
5
4.5
4
3.5
3
Vp/Vs
0
−20
−40
−60
−80
−100
−120
−140
−160
Depth (km)
−140
−100
−60 km
1.9
1.8
1.7
1.6
1.5
X (km)

Figure 4

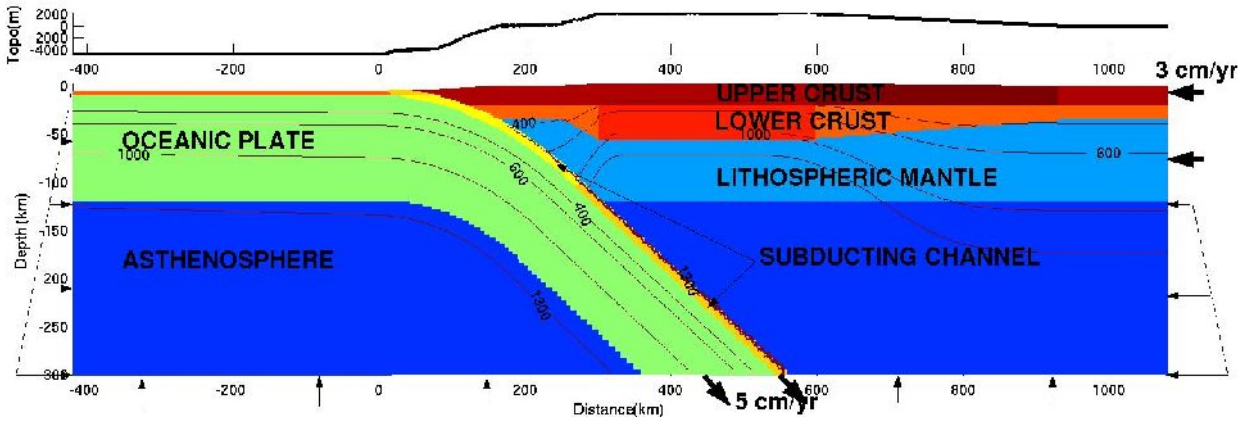
Topo(m)
2000
0
-2000
-4000
-400
-200
0
200
400
600
800
1000
3 cm/yr
UPPER CRUST
LOWER CRUST
OCEANIC PLATE
LITHOSPHERIC MANTLE
ASTHENOSPHERE
SUBDUCTING CHANNEL
Depth (km)
Distance(km)
5 cm/yr

Figure 5

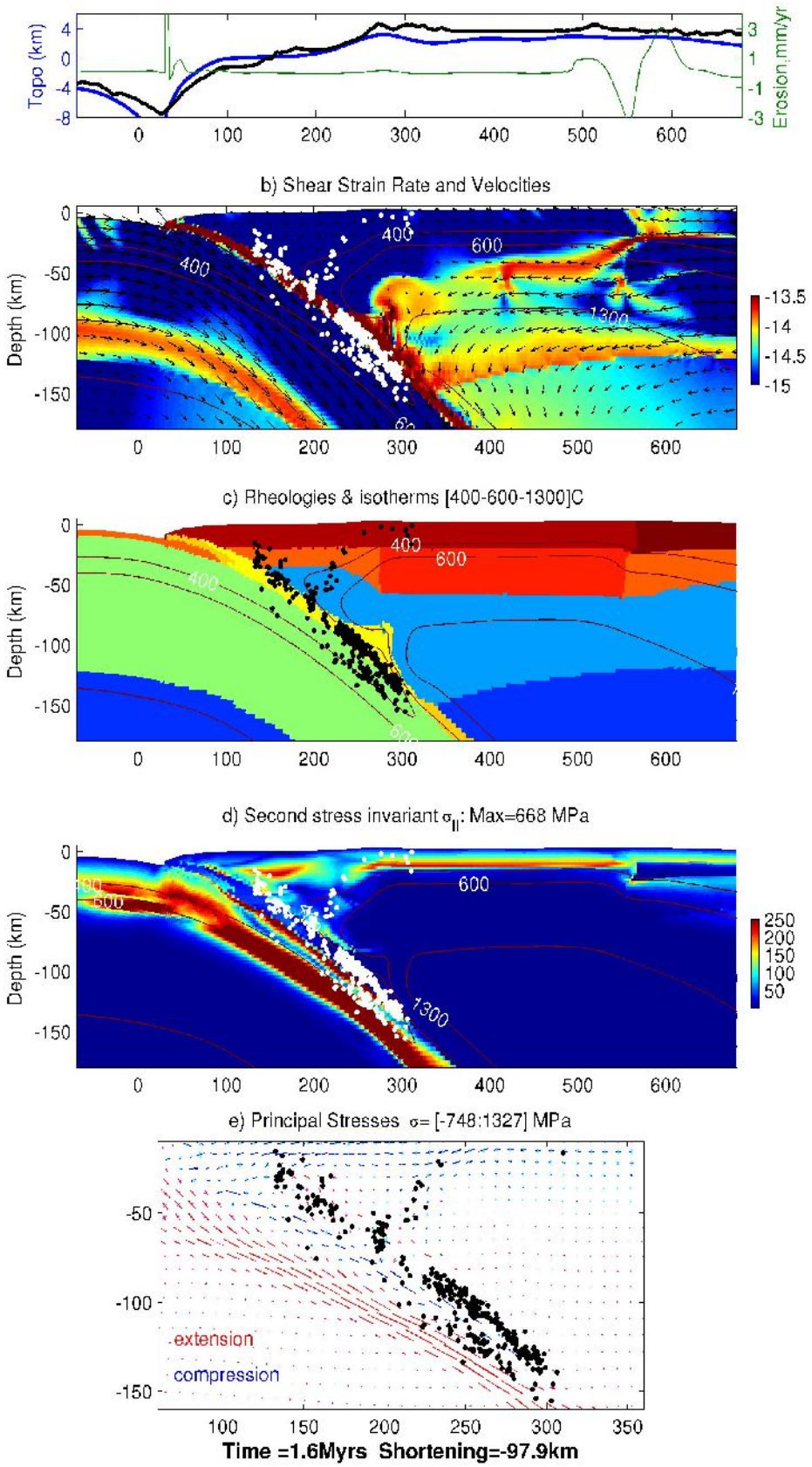
Topo (km)
Erosion,mm/yr
b) Shear Strain Rate and Velocities
Depth (km)
400
600
1300
c) Rheologies & isotherms [400-600-1300]C
d) Second stress invariant σII: Max=668 MPa
e) Principal Stresses σ= [-748:1327] MPa
extension
compression
Time =1.6Myrs Shortening=-97.9km

Figure 6

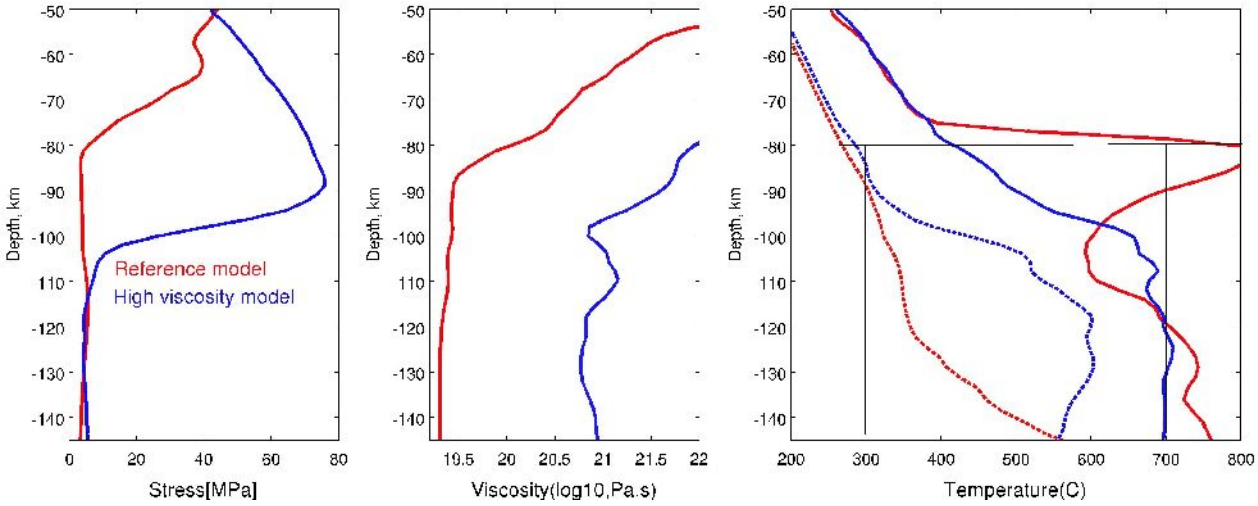
Depth, km
-50
-60
-70
-80
-90
-100
-110
-120
-130
-140
Reference model
High viscosity model
0
20
40
60
80
Stress[MPa]
19.5
20
20.5
21
21.5
22
Viscosity(log10,Pa.s)
200
300
400
500
600
700
800
Temperature(C)

Figure 7 -abc

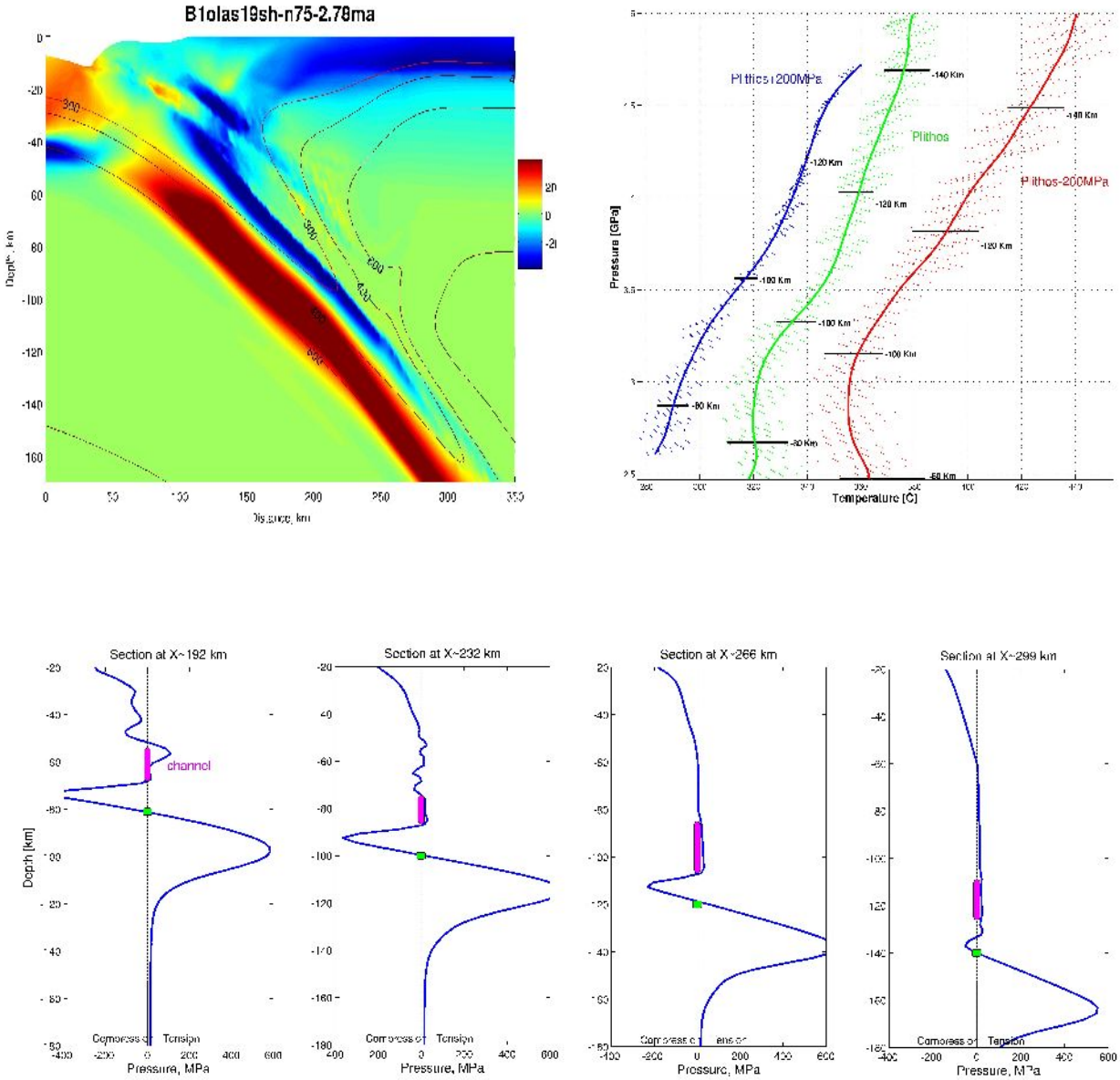
B1olas19sh-n75-2.78ma
Plithos1200MPa
Plithos
Plithos-200MPa
Pressure [GPa]
Temperature [C]
Section at X~192 km
Section at X~232 km
Section at X~266 km
Section at X~299 km
channel
Depth [km]
Pressure, MPa
Tension

Figure 8 - abc

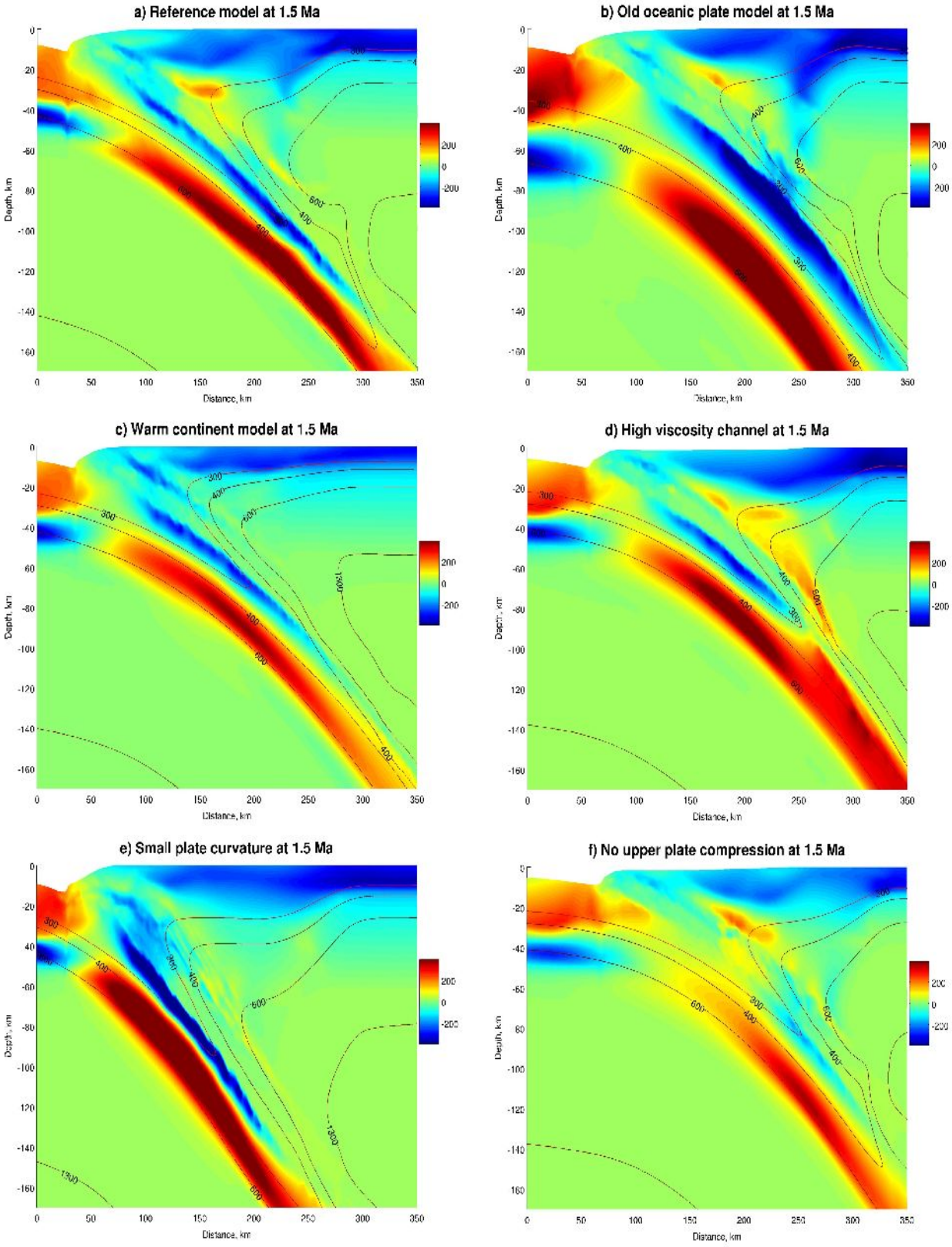
a) Reference model at 1.5 Ma
b) Old oceanic plate model at 1.5 Ma
c) Warm continent model at 1.5 Ma
d) High viscosity channel at 1.5 Ma
e) Small plate curvature at 1.5 Ma
f) No upper plate compression at 1.5 Ma
Depth, km
Distance, km

Figure 9

APPENDICES

Appendix 1: Checking the robustness of the solution.

(A) The square root of the derivative weight sum (DWS) for P waves and (B) for S waves along profile P2.

Vp (C) and Vs (D) models obtained starting from the final 1D model (red dots, Figure 2).

Vp (E) and Vs (F) models obtained starting from the initial model (blue dots, Figure 2).

We see that the influence of the initial velocity model is minor.

Appendix 2: Three resolution tests performed to study the resolution of our inversion for Vp.

Checkerboard test: (A) P wave input perturbation model, consisting of patches of 2 nodes with velocities +/- 5% compared to the normal starting model. (B) recovered perturbation model. This test highlights the fine resolution of the features in the studied DSZ area.

Restoring resolution test: (C) P wave input velocity model, which is the inverted true model. (D) recovered velocity model. The velocity features in the subduction zone are well recovered in place and magnitude. This test shows that if the observed anomalies exist, the dataset enables to recover them.

Synthetic test of a velocity model without any velocity anomaly. (E) P wave input velocity model. (F) recovered velocity model. This test shows that, if no anomaly exists, our data does not generate it.

Appendix 3 : Same as Appendix 2 for S waves.

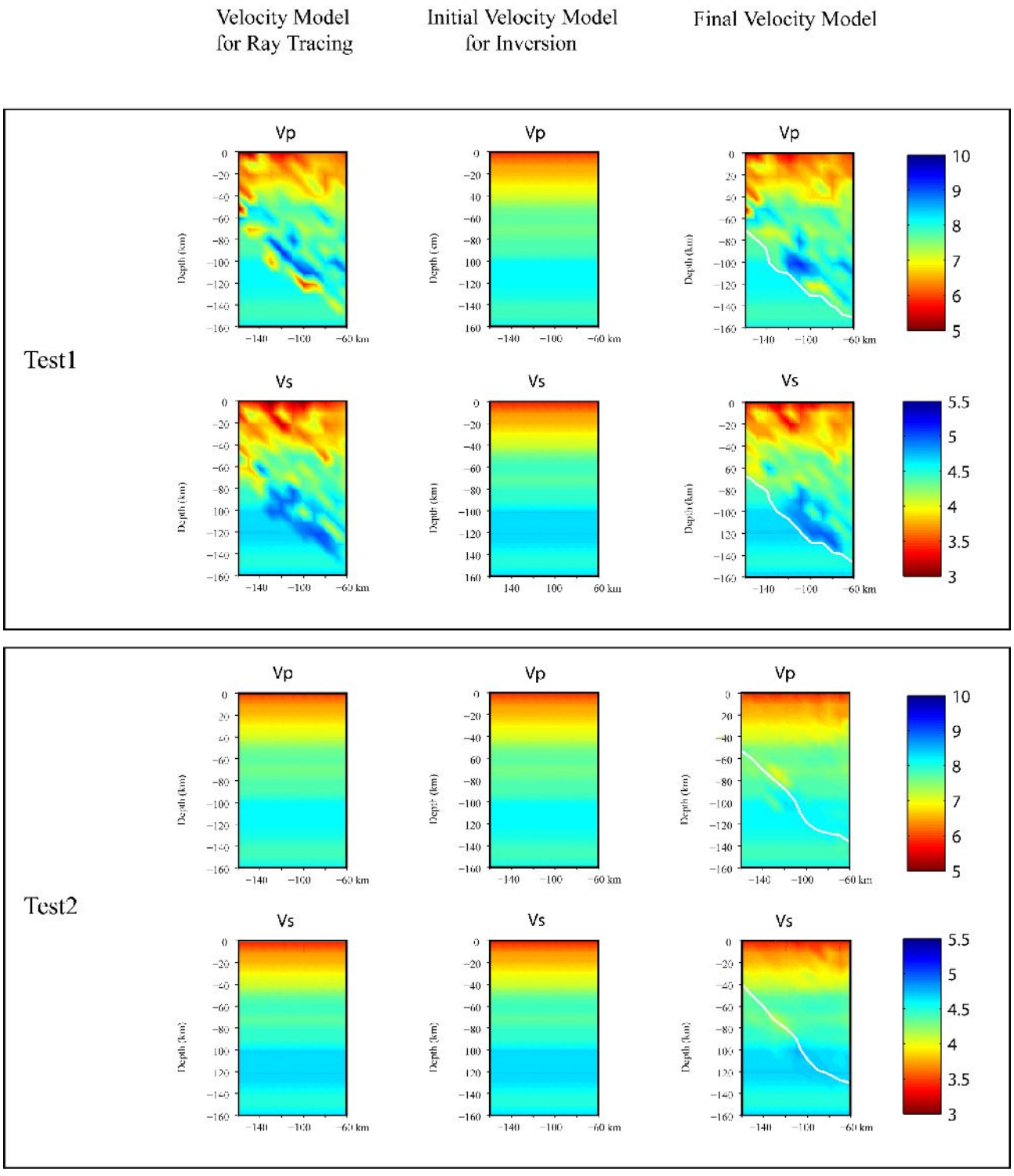
Velocity Model for Ray Tracing
Initial Velocity Model for Inversion
Final Velocity Model
Test1
Test2
Vp
Vs
Depth (km)
−140
−100
−60 km
10
9
8
7
6
5
5.5
5
4.5
4
3.5
3

Appendix 4: Thermo-mecanical markers procedure for tracking pressure and temperature.

Remeshing in Lagrangian methods is a common source of numerical diffusion, that the use of passive markers diminish, but cannot completely inhibit (e.g. Yamato et al., 2007). In Parovoz like in other FLAC methods (Cundall & Board, 1988), stresses and strains are computed at each time-step on the triangle sub-elements of the mesh (each element is made of 2 superimposed pairs of triangles that allow accurate calculation of stress and strain components), and temperatures and velocities are nodal values). At the onset of the run, we inserted 9 regularly spaced markers in each mesh element, that passively move with the Lagrangian grid during normal computation, and carry linearly interpolated, elementary stresses and temperatures. All 9 markers of a same element are assigned identical element material properties, grouping density, conductivity, and rheological parameters, represented by a colour "phase" in the setup Figure 5. When the angle of any triangular element becomes smaller than a critical value, set to 13°here, remeshing occurs and a new regular mesh replaces the old one. Then, the markers are counted in each new element, in order to identify the dominant material properties ("phase") that composes it. During remeshing, markers are also used to evaluate sub-element stress components (and therefore, pressure): new stress components are averaged over that of all markers located inside the new sub-element. For temperature, new nodal and markers temperatures are linearly interpolated from the old nodal mesh.

In Figure 8b, we plot markers values in the pressure neutral plane of the slab (Plithos in green), and in the plane located 200 MPa above and below (Plithos+200MPa in blue and Plithos-200MPa in red respectively), within a ±15 MPa range. Coloured dots are markers, coloured lines show averaged local values, and black lines indicate depth zone. We see that markers of a same colour and at similar depths follow inclined straight patterns, that correspond to markers belonging to a same sub-element: since pressure is an elementary value, markers thus have constant pressure, but slightly different lithostatic pressure because they are located at different depths (within the ±15 MPa interval). On the other hand, markers temperatures are interpolated from nodal values, and therefore do not present such artificially grouped patterns. We see that temperatures vary, at given depth, by about 20°C (horizontal extent of dots): this value is constrained by our choice of the ±15 MPa pressure interval. If we took a smaller pressure interval, then "holes" would appear at certain depths zones, because there would be no markers of that pressure range, in that zone. These "holes" are typically 2 to 3 km wide, equal to the mesh resolution there. At a given depth, the three coloured lines show a relative pressure offset of 200 MPa (as prescribed), and a temperature difference of about 30°C, which is greater than the 20°C range that individuates each pressure range (width area of same colour dots on Figure 8b). Consequently our mesh resolution allows to differentiate these three domains.